INTERNATIONAL JOURNAL FOR INNOVATION EDUCATION AND RESEARCH
ISSN: 2411-2933

Journal URL: https://scholarsjournal.net/index.php/ijier

DOI: https://doi.org/10.31686/ijier.vol10.iss12.4027

Bacterial nanocellulose and long-chain fatty acids interaction: an *in silico* study

Vinícius Rodrigues Oviedo[1*], Mariana Zancan Tonel[1], Walter Paixão de Souza Filho[1], Luiz Fernando Rodrigues Jr.[2], Michelle Rorato Sagrillo[1], Solange Binotto Fagan[1], Liana da Silva Fernandes[1]

[1] Nanosciences Post-Graduation Program, Franciscan University (UFN)

[2] Biomedical Engineering Department, Franciscan University (UFN)

Abstract

Chronic wounds are a big challenge in contemporary society, as they lead to a decrease in life-quality, amputations and even death. Infections and biofilm formation might occur with chronic wounds, due to the higher susceptibility to antibiotic multi-resistant bacteria. In this situation, novel wound dressing biomaterials are needed for treatment. Thus, the aim of this research was to evaluate a possible BNC interaction with tucumã oil/butter-derived fatty acids, as this system could be a promising biomaterial for wound treating. The interaction between cellobiose (BNC basic unit) and four fatty acids was evaluated by ab initio simulations and density functional theory (DFT), through SIESTA code. Molecular docking was also used to investigate the effect of a possible releasing of the studied fatty acids to the quorum-sensing proteins of Pseudomonas aeruginosa (gram-negative bacterium) and Staphylococcus aureus (gram-positive bacterium). According to ab initio simulations, the interaction between cellobiose and fatty acids derived from tucumã oil/butter was suggested due to physical adsorption (energy around 0.17-1.33 eV) of the lipidic structures into cellobiose. A great binding affinity (ΔG ranging from 4.2-8.2 kcal.mol^{-1}) was observed for both protonated and deprotonated fatty acids against P. aeruginosa (LasI, LasA and Rhlr) and S. aureus (ArgA and ArgC) quorum-sensing proteins, indicating that these bioactive compounds might act as potential antimicrobial and/or antibiofilm agents in the proposed system. Hence, from a theoretical viewpoint, the proposed system could be a promising raw biomaterial in the production of chronic wound dressings.

Keywords: bacterial cellulose; tucumã; *Astrcaryum vulgare*, *ab initio*, DFT, docking.

1. Introduction

Skin is the largest organ of the human body and is responsible for several biological functions, such as: (i) serving as an external barrier for pathogens, (*ii*) the maintenance of humidity and temperature of adjacent tissues, (*iii*) water secretion, and so forth (Bacakova et al., 2020). In this sense, chronic wounds are known to affect about 70 million people worldwide, thus being a major problem in contemporary society (Xiao, Ahadian, & Radisic, 2017), as they can lead to a decrease in life-quality, amputations, and even death (Homaeigohar & Boccaccini, 2020). Hence, chronic wounds are commonly associated with expensive costs in healthcare systems (Olsson et al., 2019). In brief, a chronic wound is defined as a wound that heals in an unpredictable

time span, which can result in improper healing and further complications, such as infections (Nethi, Das, Patra, & Mukherjee, 2019). Some common chronic wounds are pressure ulcers, vascular ulcers (which include venous and arterial ulcers) and diabetic ulcers (Frykberg & Banks, 2015). Chronic wounds are caused by persistent diseases and aging (L. Gould et al., 2015; X. Zhang et al., 2020).

The wound healing process has three main phases: haemostasis, inflammation and proliferation (Kanikireddy, Varaprasad, Jayaramudu, Karthikeyan, & Sadiku, 2020). The aim of haemostasis is to stop bleeding by platelet accumulation and cloth formation. The inflammation is guided by vasodilatation in the wound area and by macrophage action to attack pathogens and remove apoptotic cells. During proliferation, a new connective tissue, composed of extracellular matrix (ECM) and collagen, is formed, followed by tissue remodelling and tensile strength improvement (Nethi et al., 2019). However, all these physiological processes tend to take more time than usual and are more susceptible to complications in a chronic wound (Cai et al., 2018; Shahi, Singh, Kumar, Gupta, & Singh, 2013).

When a patient has a chronic wound, they are highly susceptible to infections and complications associated with drug-resistant bacteria (Y. Wang et al., 2019), thus needing novel approaches to the treatment. The main bacteria responsible for chronic wound infections are *Pseudomonas aeruginosa*, *Staphylococcus aureus*, *Acinetobacter baumannii* and *Klebsiella pneumoniae* (Moghadam, Khoshbayan, Chegini, Farahani, & Shariati, 2020). Among these microorganisms, *P. aeruginosa* and *S. aureus* are classified as critical and high priority by the World Health Organization (Asokan, Ramadhan, Ahmed, & Sanad, 2019), respectively, as they require novel effective antimicrobial agents.

In addition to infections, bacteria can normally produce biofilms (polysaccharide-based barriers) on the wound as a protection mechanism, which is guided by a process called *quorum-sensing* (QS) (Subramani & Jayaprakashvel, 2019). It is estimated that these biofilms are present in about 60% of chronic wounds (Teixeira, Paiva, Amorim, & Felgueiras, 2020). QS refers to the way in which bacteria communicate with each other to increase populational density and to produce biofilms (Gnanendra, Anusuya, & Natarajan, 2012; Papenfort & Bassler, 2016). This communication occurs through signalling substances, known as auto-inducers, such as *N*-acyl-homoserine lactones (AHL), autoinducing peptides (AIP) and auto-inducers II (A-2) mainly (An et al., 2019; Huang et al., 2016). Therefore, the often-investigated approaches to combat bacterial infections and biofilm production rely on what is called *quorum-quenching* (QQ), that is, mechanisms able to interfere or even interrupt the QS process (Rehman & Leiknes, 2018).

At the same time, bacterial nanocellulose (BNC) is an exopolysaccharide produced by acetic bacteria that can be used as a dressing intended for chronic wounds (Cavalcanti et al., 2017; Portela, Leal, Almeida, & Sobral, 2019). Due to its nanofibrous structure (fibre diameters ranging from 20-100 nm (Abol-Fotouh et al., 2020; Jozala et al., 2016; Norrrahim et al., 2021; Oviedo et al., 2021)), BNC displays unique properties, such as: (*i*) the absence of lignin, pectin and hemicellulose phases; (*ii*) a high degree of crystallinity; (*iii*) biocompatibility; (*iv*) no toxicity; (*v*) a high surface to mass ratio; and (*vi*) a high water absorption ability, among others (Choi & Shin, 2020; Gorgieva, 2020; SALIHU et al., 2019). Due to its outstanding properties, BNC-based wound dressings can serve as mechanical barriers to external microorganisms, maintain the humidity of the target area, absorb a great amount of wound exudate, present gas/liquid permeation, and display a suitable tensile

strength (Azeredo, Barud, Farinas, Vasconcellos, & Claro, 2019). Also, when applied to treat severe burns, BNC provides pain relief to patients, due to the protection of the nerve endings (Pang et al., 2020). Despite the features of BNC, it lacks antimicrobial activity in the pristine form (El-Wakil, Hassan, Hassan, & El-Salam, 2019); to solve this, several antimicrobial agents could be attached to the BNC structure by *ex situ* or *in situ* modifications (Stumpf, Yang, Zhang, & Cao, 2018).

Both synthetic and natural antimicrobial agents have been investigated in the literature (Varier et al., 2019). The preference for naturally-derived antimicrobial agents in biomedical applications relies on the fact that microorganisms cannot generate resistance to them as they are natural substances (Kumar, Lee, Beyenal, & Lee, 2020). Naturally-derived antimicrobial agents include vegetal and essential oils, antimicrobial peptides and fatty acids (Aslanli, Lyagin, Stepanov, Presnov, & Efremenko, 2020; Casillas-Vargas et al., 2021; Lalouckova et al., 2021; Pereira dos Santos et al., 2019; Sekar, Paul, Srinivasan, & Rajasekaran, 2021). In this respect, tucumã (*Astrocaryum vulgare*), an Amazon fruit from which an oil or a butter can be extracted, and its derivatives have been investigated for biomedical applications (Baldissera et al., 2017; Bressa et al., 2021; Cordenonsi et al., 2020; Fernandes, 2015; Rossato et al., 2020, 2021). The high fatty acids content of tucumã is the main feature that can provide either antimicrobial or antibiofilm activity to its derivatives (Casillas-Vargas et al., 2021).

Besides the structural role of fatty acids, they are also known to play a protective role in both humans and plants (Badhe, Gupta, & Rai, 2019; Cartron et al., 2014; Lim, Singhal, Kachroo, & Kachroo, 2017; Santos et al., 2021). Moreover, fatty acids have been found to display antibiofilm properties in low concentrations and antimicrobial activity in high concentrations (Kumar et al., 2020). It is also worth mentioning that fatty acids are amphiphilic substances that form and/or can mimic the QS structures of pathogenic bacteria, such as diffusive signal factors (DSF) and AHL, for example (Dow & Naughton, 2017; Espinosa-Urgel, 2016). The main hypotheses of the antimicrobial/antibiofilm activity of fatty acids are: (*i*) the undesirable release of metabolites of intracellular pathogens by cellular membrane disruption; (*ii*) nutrient absorption blockage, as well as a negative influence on the electron transport chain; and (*iii*) toxicity caused by their oxidation by-products (Kumar et al., 2020).

Tucumã oil and tucumã butter have already been evaluated in the literature and presented good biocompatibility, an ability to modulate the inflammatory process and a 60-day storage stability, as well as antimicrobial and antibiofilm activity against pathogenic bacteria (Rossato et al., 2021). In addition, the combination of tucumã oil and butter together resulted in an improved healing activity of HFF-1 cells (human fibroblasts) using scratch *in vitro* tests (Rossato et al., 2020). These interesting properties make tucumã oil and butter suitable for applications involving chronic wound dressings. Also, the abundance of tucumã and the presence of other components in its structure that are known to be responsible for anti-inflammatory and antioxidant properties, such as beta-carotene, polyphenols and tocopherols, can be beneficial for the purpose of chronic wound dressings. To the best of our knowledge, tucumã oil and butter impregnation into BNC has not been studied yet, either *in silico* or *in vitro*.

In silico methods, such as *ab initio* simulations and molecular docking, could be useful during the proposition of novel wound dressing materials, as these simulations are in accordance with the 3R principles (replacement,

reduction and refinement) (Jean-Quartier, Jeanquartier, Jurisica, & Holzinger, 2018). The interaction of biopolymers and hydrogels with other chemical compounds has already been investigated through *ab initio* simulations based on the density functional theory (DFT) (Cortes et al., 2019; De Salvi et al., 2014; Deka & Bhattacharyya, 2017; Pontoh, Rarisavitri, Yang, Putra, & Anugrah, 2022), which can provide useful insights concerning the mechanisms of the possible modification of BNC with tucumã oil and butter.

Pontoh *et al*. evaluated the interaction between cellulose and amylum through DFT/*ab initio* simulations, in which an interaction occurred by hydrogen bond formation that could be attributed to a physical adsorption (Pontoh et al., 2022). Deka and Bhattacharyya also studied the interaction of chitosan (a biopolymer with analogous monomers of cellulose) and its derivatives with amino acids, based on DFT and *ab initio* simulations, focusing on a protein-carrier system (Deka & Bhattacharyya, 2017). In this study, the interactions between the structures were strong, being indicative of chemical adsorption, due to the amine groups present in the dimer instead of only hydroxyl groups, as in cellobiose. Likewise, Cortes *et al*. studied the interaction of acrylamide hydrogels and anti-malaria drugs through DFT/*ab initio* simulations, with a focus on drug delivery (Cortes et al., 2019). Their findings suggested a physical adsorption of the primaquine, amodiaquine and chloroquine drugs in the polymeric matrix, which was interesting for the treatment of malaria.

Besides these studies, other investigations were also published in literature involving *ab initio* simulations to study cellulose I and fatty acid properties separately. For example, Li evaluated the structural properties of cellulose I, which is the major crystalline phase of BNC (Kondo, Rytczak, & Bielecki, 2016; Y. Li, Lin, & Davenport, 2011). In an equivalent manner, Mohammed investigated the structural properties of date palm seed (DPS) extract through DFT/*ab initio* simulations using its major fatty acids (lauric, myristic, oleic, phthalic, caprylic and palmitic acids), with the goal of proposing a green anti-corrosive material. In this context, other studies have also investigated the interaction of carbon-based structures with chemical compounds through *ab initio* simulations (de Moraes, Tonel, Fagan, & Barbosa, 2019; Iuri M. Jauris, Fagan, Adebayo, & Machado, 2016; Machado et al., 2016; Ramos et al., 2018; Tonel, González-Durruthy, Zanella, & Fagan, 2019; K. Wang et al., 2020).

Additionally, molecular docking has been used to infer the antimicrobial or antibiofilm activity of potential bioactive substances due to the binding affinity of these chemical compounds to QS proteins of pathogenic bacteria (Aslanli et al., 2020; Chemmugil, Lakshmi, & Annamalai, 2019). Structures like *L*-tryptophan have demonstrated a binding affinity to four QS proteins of *P. aeruginosa*, which was accomplished with reduced *in vitro* gene expression (Chakraborty et al., 2018). Hence, assuming the releasing of BNC-modifier substances (*e.g*., tucumã oil and butter major fatty acids), the potential antimicrobial/antibiofilm activity of the proposed system could be assessed.

In this sense, the investigation and analysis of the proposed system could be enhanced by combining *ab initio* and docking simulations. This was previously shown in studies involving functionalized graphene interacting with glutamate, in which the interactions of graphene/glutamate (modifying the involved structures) were attributed to a physical adsorption regime and confirmed both by *ab initio* and molecular docking (Tonel et al., 2019).

Thereby, the aim of this paper was to investigate the interaction of BNC with tucumã oil and butter from an

in silico viewpoint, to propose a possible antimicrobial and/or antibiofilm system that could be used as the raw biomaterial for chronic wound dressing production. The investigation was based on *ab initio* simulations and molecular docking, with the hypothesis that the major fatty acids contained in the tucumã oil and butter could be used to impregnate the BNC structure and that their release might interfere with the QS process of two pathogenic bacteria, *P. aeruginosa* (gram-negative) and *S. aureus* (gram-positive).

2. Methods

First, it is important to mention that all the chemical structures were obtained from the PubChem database. Cellobiose (CID: 10712), which is the repeating unit of BNC, and the major fatty acids that compose the tucumã oil and butter precursors (~ 10% wt.) were used during simulations, due to computational limitations and to reduce computational costs. The choice of cellobiose was possible due to DFT-based studies that use this dimer to estimate interactions of nanocellulose oligomers or crystal structures with other chemical compounds (De Salvi et al., 2014; Y. Li et al., 2011; Vilela et al., 2020; Zarei, Niad, & Raanaei, 2018). Also, DFT studies involving polymers normally use dimers during the simulations (Deka & Bhattacharyya, 2017; Pontoh et al., 2022; Rahmawati, Radiman, & Martoprawiro, 2018), as it is known that the interaction between dimers and other compounds is extendable to oligomers and macromolecules (Cortes et al., 2019). The fatty acids used were: lauric acid (CID: 3893), myristic acid (CID: 11005), oleic acid (CID: 445639) and palmitic acid (CID: 985), all of which are the major components of tucumã butter, while oleic and palmitic acids for the major components of tucumã oil (COSTA, SANTOS, CORRÊA, & FRANÇA, 2016; Leonardi, Arauz, & Baruque-Ramos, 2019).

Ab initio simulations showed the electronic nature of the interaction between each fatty acid and the cellobiose. Such investigations might serve as an indication of BNC impregnation/modification with tucumã oil and butter. Likewise, molecular docking was used to assess the interaction of the studied fatty acids (the bioactive compounds of the proposed system) against three QS proteins of *P. aeruginosa* and two QS proteins of *S. aureus*. By confirming the binding affinity of the bioactive compounds of the proposed system against these macromolecules, it is anticipated that they can act as antimicrobial or antibiofilm agents.

2.1 Ab initio simulations

It is worth pointing out that *ab initio* simulations were implemented through SIESTA computational code (Soler et al., 2002) and based on the DFT, Born-Oppenheimer approximation, Hohenberg-Kohn theorems, and self-consistent Kohn–Sham equations (Born & Oppenheimer, 1927; Hohenberg & Kohn, 1964; Kapil, Shukla, & Pathak, 2020; Kohn & Sham, 1965). Also, the following parameters were used: double ζ plus a polarized function (DZP) as the numerical basis set, the local density approximation (LDA) approach to express the exchange and correlation potential (V_{xc}) (Perdew & Zunger, 1981), and the basis set superposition error (BSSE) correction (Boys & Bernardi, 1970). The LDA approximation and BSSE correction were selected due to: (*i*) both having already been used in similar works (de Moraes et al., 2019; Hernández Rosas, Ramírez Gutiérrez, Escobedo-Morales, & Chigo Anota, 2011; I. M. Jauris et al., 2016; Iuri M. Jauris et al., 2016; Machado et al., 2016); (*ii*) the LDA shows suitable agreement of bonding energies and bond distances in comparison with

experimental data; and (*iii*) LDA also displays good agreement for weak interacting systems, particularly in materials which present π-π interactions (Arrigoni & Madsen, 2019; Cresti, Lopez-Bezanilla, Ordejón, & Roche, 2011; B. Li, Ou, Wei, Zhang, & Song, 2018; Tournus & Charlier, 2005; Tournus, Latil, Heggie, & Charlier, 2005). Other relevant simulation parameters were grid cut-off = 200 Ry, residual forces < 0.05 eV.Å^{-1}, and cell dimensions of 50 Å in all directions. The structures were optimized at first; thus, their local density of states (LDOS) information was used as a basis to produce possible configurations for fatty acids/cellobiose interactions. The following were obtained in each interacting system: (*i*) BSSE-corrected interaction energy; (*ii*) distance of closed interacting atoms; (*iii*) Highest Occupied Molecular Orbital (HOMO) -Lowest Unoccupied Molecular Orbital (LUMO) difference (ΔHL); and (*iv*) charge transfer between the structures. The BSSE-corrected interaction energy was calculated through Equation 1 and expressed in eV. This type of methodology has been used in recent studies within our research group (de Oliveira et al., 2020; Ramos et al., 2018; Tonel et al., 2019). The subscript *ghost* in Equation 1 means the atomic basis set for atomic positions of A and B, but without representing the atomic potentials in such positions (Ramos et al., 2018). It is worth to mention that all the fatty acids were used in the protonated state.

$$E_{BSSE} = E_{System} - E_{(A+B(ghost))} - E_{(A(ghost)+B)} \quad (1)$$

2.1 Molecular docking

Molecular docking was used to investigate the interaction between the major fatty acids of tucumã oil and butter and the proteins that participate in QS of *P. aeruginosa* (gram-negative bacterium) and *S. aureus* (gram-positive bacterium). The following macromolecules were obtained from the Protein Data Bank (PDB): LasI (PDB ID: 1RO5), LasA (PDB ID: 3IT7) and RhlR (PDB ID: 6CC0) – *P. aeruginosa*; AgrA (PDB ID: 4G4K) and AgrC (PDB ID: 4BXI) – *S. aureus*. During docking simulations, AutoDock Tools was used for protein and ligand preparation, and AutoDock Vina was used to perform the docking itself. In the case of 4BXI, which presented missing amino acid residues, protein homology modelling was used through the Swiss-Model platform before docking. The modelled protein was validated through a Ramachandran plot (Hema, Ahamad, Joon, Pandey, & Gupta, 2021), in which more than 96% of protein amino acid residues were located in favourable regions. The Ramachandran plot for 4BXI homologue protein and the grid box information are available in the Supplementary Material.

Notably, LasI and LasA proteins play active roles in the Las and Rhl QS-systems of *P. aeruginosa*, in which LasI and LasA are responsible for the bacterial gene transcription associated with biofilm production (A. Gould et al., 2004). Likewise, AgrA and AgrC also play active roles in the Agr QS-system of *S. aureus*, being the two proteins responsible for virulence factor expression, extracellular toxin release and repression of adhesins (Leonard, Bezar, Sidote, & Stock, 2012).

The molecular docking protocol developed by Forli and colleagues (Forli et al., 2016) was used with adaptations, such as: (*i*) the platform DeepSite was used to predict the active site of the QS proteins; and (*ii*) the eBoxSize script was used to calculate the box dimensions according to ligand sizes (Feinstein & Brylinski, 2015; Lopreiato et al., 2021; Schopf et al., 2021). The visualization steps and the analysis of results were

performed using PyMol (3D visualization) and LigPlus (2D visualization). The binding affinity (which approximates to the free energy of binding (FEB) of each interaction) between protein-ligand was calculated using Equation 2 and expressed in kcal.mol^{-1}, where more negative values indicate great protein-ligand complex affinity (due to the spontaneity to bind), while positive values indicate the absence of affinity, characteristic of an unfavourable docking result.

$$\Delta G \approx FEB = \Delta G_{vdW} + \Delta G_H + \Delta G_e + \Delta G_{int} \quad (2)$$

where:

ΔG: protein-ligand complex binding affinity.

ΔG_{vdW}: chemical potentials related to Van der Waals interactions.

ΔG_H: chemical potentials related to hydrogen bonding.

ΔG_e: chemical potentials related to electrostatic interactions.

ΔG_{int}: chemical potentials related to intramolecular interactions.

Another import docking metric, the Root Mean Squared Deviation (RMSD), was used together with the binding affinity during the analysis of results. The RMSD is given by Equation 3, and the docking results in which RMSD < 2.0 Å and RMSD ≠ 0 Å were considered favourable docking runs, serving as a validating approach (Schweiker & Levonis, 2020; Trott & Olson, 2009).

$$RMSD(pose_{ilig}, pose_{irec}) = \sqrt{\frac{\sum_n (atom_{(lig)} - atom_{irec})^2}{n}} \quad (3)$$

where:

atom$_{(ilig)}$: mean ligand atomic position.

atom$_{(irec)}$: mean receptor (protein) atomic position.

n: mean system atomic position.

It is important to mention that the docking analyses were validated by applying the same protocol for *L*-tryptophan (CID: 6305) and anethol (CID: 637563), which were used as control compounds, as they were already capable of eliciting the QQ on proteins of *P. aeruginosa* and *S. aureus* (Chakraborty et al., 2018; Kwiatkowski et al., 2019), respectively, from an *in silico* and/or *in vitro* viewpoint. After that, the influence of using the fatty acids in the protonated and deprotonated forms were evaluated, where the latter tends to occur with pH values above 7.4 (Shoemark et al., 2021). Studying the two fatty acid protonation states is pertinent to the clinical viewpoint. Succinctly, a healthy skin pH (pH = 4.0 – 6.0) is characterized as slightly acidic, while chronic wounds normally present pH = 7.15 – 8.30, which tend towards alkalinity (Gethin, 2007; Jones, Cochrane, & Percival, 2015). In this context, the protonation state of the bioactive compounds of the proposed system is indispensable in molecular docking simulations, as wound dressings do not elicit skin pH changes in normal conditions, while pH changes are possible in chronic wound treatment and might be beneficial to the patient (Jones et al., 2015).

The statistical methods used a 95% confidence interval and involved: (*i*) descriptive statistics and contingency tables (expressed in heatmaps), used to deal with more punctual investigations (*e.g.*, the influence of fatty acid deprotonation on the residual amino acids involved in the interaction with QS proteins, as well as the changes

in the nature of the interactions); (*ii*) Chi-Squared test, intended for hypothesis testing validation. All statistical analyses were performed through *Python 3.8* using the Google Colab platform.

3. Results and discussion

3.1 Ab initio simulation

As mentioned previously in the Methods section, the LDOS information was obtained for all the studied structures; that is, their HOMO and LUMO information, as well as the HOMO/LUMO difference (ΔHL). Table 1 shows the quantitative results obtained for isolate structures. Likewise, Figure S1 (Supplementary Material) presents the LDOS plots for the studied structures.

Table 1. HOMO and LUMO difference (ΔHL) for isolated structures.

Structure	ΔHL (eV)	ΔHL found in literature (eV)	Reference
Cellobiose	5.44	5.40	[59]
Lauric Acid	5.29	5.28	[102]
Myristic Acid	5.28	5.29	[102]
Oleic Acid	4.72	4.55	[102]
Palmitic Acid	5.27	5.29	[102]

As can be seen in Table 1, the overall results were close to those of the literature studies (Y. Li et al., 2011; Mohammed, Othman, Taib, Samat, & Yahya, 2021), although oleic acid presented a difference to the literature, which could be attributed to the unsaturated carbon chain and the fact that Mohammed *et al*. used a GGA approximation in their study (Mohammed et al., 2021). According to Figure S1, the LDOS plot of the cellobiose HOMO presented charges mainly distributed on the first glucopyranose ring, as well as on the hydroxyl groups along the structure. Meanwhile, the cellobiose LUMO displayed charges on the second glucopyranose ring and along the carbons and hydroxyls. Also based on Figure S1, the saturated fatty acid (lauric, myristic and palmitic acid) charges were mainly located at the carboxylic acid function group (COOH) in both the HOMO and LUMO. On the other hand, oleic acid had the charges distributed on the unsaturated region (C=C) of the carbon chain in the HOMO plot, and distributed between the COOH and C=C regions in the LUMO plot. These results were in accordance with literature studies involving DFT and these fatty acids (Ituen, Essien, Udo, & Oluwaseyi, 2014; Mohammed et al., 2021; K. Wang et al., 2020).

The LDOS plots illustrated in Figure S1 served as the basis for the evaluation of the possible interactions between cellobiose and each fatty acid. Based on the LDOS plots, several configurations were elaborated to investigate possible interactions between cellobiose and fatty acids. Figure 1 shows one example for these

configurations: the cellobiose-lauric acid interaction. Other configurations for cellobiose interaction with myristic acid, palmitic acid and oleic acid are available in the Supplementary Material (Figure S2).

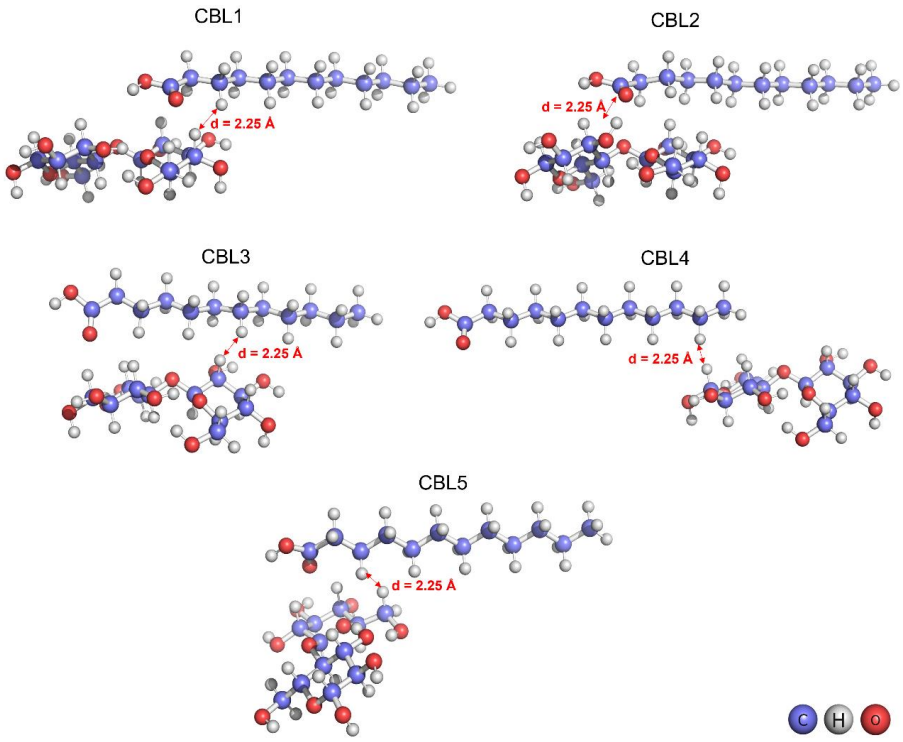

Figure 1. Configurations for the interaction of cellobiose-lauric acid. (CBL refers to cellobiose-lauric acid system, while the numbers refer to configuration id).

Table 2 shows the results obtained for all cellobiose-fatty acid systems. It is important to observe that the absolute values for ΔHL were less than those for the isolated structures, shown in Table S1. This behaviour suggests that these structures might interact when in contact with each other, as compounds with low ΔHL have low thermodynamic stability and high reactivity (Miar, Shiroudi, Pourshamsian, Oliaey, & Hatamjafari, 2021; Pontoh et al., 2022; G. Zhang & Musgrave, 2007). This happens because removing an electron from the HOMO and adding it to the LUMO is an energetically favourable process in a compound with low ΔHL and is energetically unfavourable in compounds with higher ΔHL (Ruiz-Morales, 2002). Looking at the obtained (*i*) binding energy, (*ii*) distances of the closed atoms, and (*iii*) charge transfer values, a physical adsorption could be seen between the cellobiose unit and each fatty acid in all configurations [56–58, 65, 81]. In practical terms, the physical adsorption indicates that these cellobiose-fatty acid configurations might occur at room temperature, and they can be broken by physical stimuli, like an increase in temperature, pressure conditions, humidity, pH, contact with other compounds and so forth (Kecili & Hussain, 2018). Furthermore, the physical interaction is pertinent to the research purpose, once it seeks to release the bioactive compounds incorporated into the polymeric cellulose matrix.

Overall, it was noted that the binding energies were greater when the LDOS regions with high charges were closer together. Similarly, when these regions moved apart, a lower binding energy was obtained. Lauric, myristic and palmitic acids interacted with cellobiose in a similar manner, as they are saturated fatty acids that

differ in the size of their carbon chain. Oleic acid was the only unsaturated fatty acid in this research, and the two regions of the LDOS plots led to different configurations when compared to the cellobiose-saturated fatty acid systems. However, in the cellobiose-oleic acid interactions, the values for (*i*) binding energies, (*ii*) distances between the closed interacting atoms, and (*iii*) charge transfer also suggest an interaction based on physical adsorption [56–58, 65, 81]. Figure 2 illustrates the energy level plot and the LDOS plot for the most stable cellobiose-lauric acid and cellobiose-oleic acid systems. It can be inferred that the difference in ΔHL in relation to the isolated structures ranged from 0.28-1.50 eV, which is in accordance with literature studies that also attributed the interactions to physical adsorption [53, 57, 59, 60, 72].

Table 2. Results for cellobiose-fatty acid interacting systems.

Configuration	Binding energy* (eV)	Molecular distance** (Å)	ΔHL (eV)	Charge transfer*** (e^-)
CBL1	-0.55	2.04	4.47	0.04
CBL2	-0.78	1.70	3.94	0.05
CBL3	-0.67	2.01	4.25	0.03
CBL4	-0.17	2.18	4.97	0.11
CBL5	-0.27	2.25	4.39	0.08
CBM1	-0.49	1.57	3.74	-0.03
CBM2	-0.57	1.76	4.27	-0.01
CBM3	-1.09	1.84	4.04	0.01
CBM4	-0.96	1.79	4.85	0.05
CBM5	-1.33	1.89	4.77	0.03
CBP1	-1.21	1.94	4.92	0.13
CBP2	-0.27	2.14	4.91	0.03
CBP3	-0.41	2.08	4.99	0.03
CBP4	-0.33	1.96	4.98	0.02
CBP5	-0.33	2.13	4.50	0.02
CBO1	-0.25	2.42	4.63	0.04
CBO2	-0.43	1.84	4.52	0.03
CBO3	-0.38	2.02	4.70	0.02
CBO4	-0.48	1.93	4.34	0.01

* The negative sign indicates attractiveness between the structures.

** Distances are in relation to the closest atoms of the two structures interacting.

*** In relation to cellobiose. Positive values indicate charge receipt; negative value indicate charge donation.

All the fatty acids were in the protonated state.

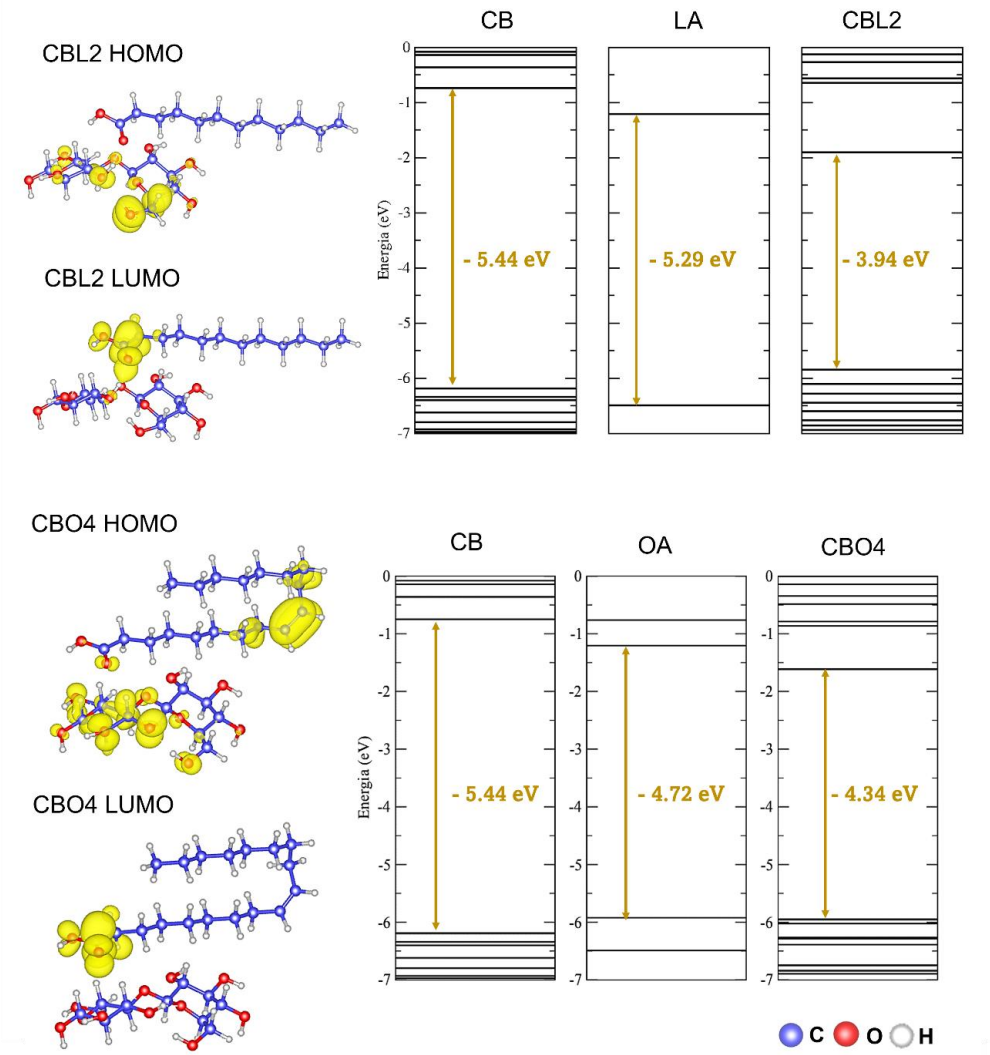

Figure 2. Energy levels and LDOS plots for the most stables systems of cellobiose-lauric acid and cellobiose oleic acid (isosurface values of 0.001 e^-/Borh^3).

Based on the *ab initio* results and the suggested physical adsorption, the studied fatty acids were then used to investigate their own effect against macromolecules of *P. aeruginosa* and *S. aureus* through molecular docking. It is noteworthy that this effect could be beneficial to the proposed system due to the hypothesis that these fatty acids could be desorbed from cellobiose and possibly promote the QQ of pathogenic bacteria.

3.2 Molecular docking

The binding affinities obtained from favourable molecular docking runs (RMSD < 2.0 Å and RMSD ≠ 0 Å) for the tucumã oil and butter major fatty acids against the QS proteins of *P. aeruginosa* and *S. aureus* are shown in the Supplementary Material (see Tables S2 and S3). It is interesting to note that all the ligands presented interesting ΔG values during interaction with the QS proteins, either in the protonated or deprotonated form, in which more negative signs indicates good spontaneity of binding (Schweiker & Levonis, 2020). Figure 3 exemplifies two complexes obtained during docking simulations: 6CC0-oleic acid (*P. aeruginosa*) and 4BXI-myristic acid (*S. aureus*), respectively. A hydrogen bond could be seen in the 6CC0-

oleic acid interacting complex between oleic acid and the Val78 amino acid residue (bond length 2.89 Å), as well as hydrophobic contacts with other amino acid residues of the 6CC0 protein. Correspondingly, a hydrogen bond between myristic acid and the Thr21 amino acid residue (bond length 3.22 Å) and hydrophobic contacts with other amino acid residues of the 4BXI protein were observed in the 4BXI-myristic acid interacting complex.

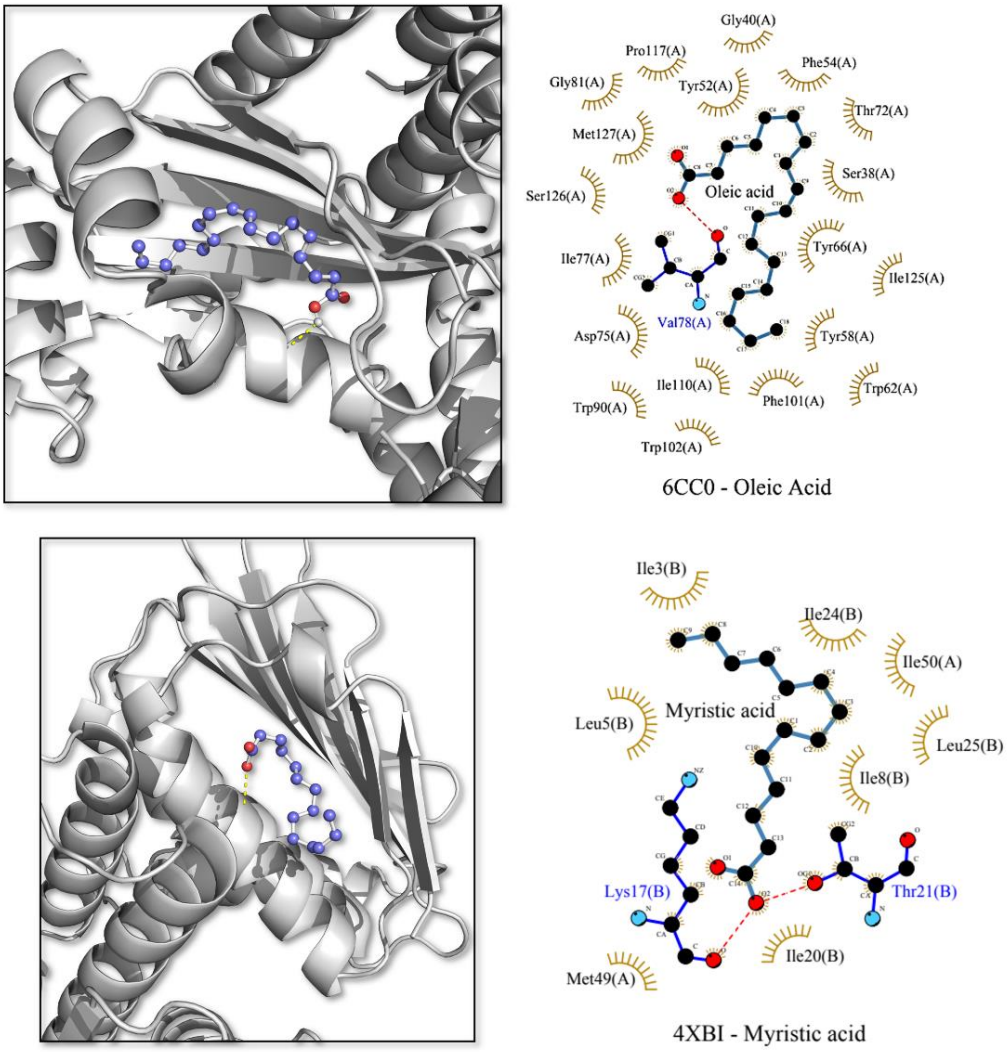

Figure 3. 6CC0-oleic acid (top) and 4BXI-myristic acid (bottom) complexes.

The validation of molecular docking simulations is shown in Table 3. As mentioned in the Methods section, the binding affinities and amino acid residues involved in the interaction between each protein and the studied fatty acids were compared to the best pose of the controls (Nogueira et al., 2021). Based on Table 3 and the Supplementary Material (Tables S2 and S3), it was possible to note that the binding affinities of the fatty acids against *P. aeruginosa* and *S. aureus* proteins were close to those of the controls. Moreover, the percentage of amino acid residues that were common to both the fatty acids and the controls suggest a similar behaviour compared to *L*-tryptophan and anethol, despite the 4G4K protein presenting a lower percentage (50%) of amino acid residues in common between the studied fatty acids and the controls. This percentage was relevant

for the other proteins, which suggests that the interacting site was similar for the tucumã oil/butter major fatty acids and the control compounds (Nogueira et al., 2021). As the majority of the amino acid residues involved in the fatty acid/QS protein interactions are practically the same as the controls, it is inferred that these structures could present antibiofilm or antimicrobial activity against *P. aeruginosa* and *S. aureus* from a practical viewpoint (Chakraborty et al., 2018; Kwiatkowski et al., 2019). However, in some cases, such as 1RO5, an amino acid residue (*e.g.*, Ile107) might still interact through a nonpolar contact rather than a polar one, which was found in the *L*-tryptophan ligand and also happened in the case of 6CC0, where the Tyr66 residue also appeared in the fatty acid/6CC0 interactions, but by a nonpolar contact instead of a polar one. For these two situations, as well as in the case of protein 4G4K, it is supposed that the inhibition of the QS protein might still happen, but due to a mechanism not fully understood yet.

Protein	**Binding affinity (kcal.mol^{-1})**	**Contact**	**Aminoacid residues**	**Residues involved in the interaction with all fatty acids**	**%Residues in common***
1R05	-5.8	Polar	Ile107	Ala106, Arg30, Ile107, Phe27, Phe105, Phe117, Thr144	70%
		Apolar	Ala106, Arg30, Phe27, Phe105, Phe117, Thr144, Thr145, Trp33, Val126		
3IT7	-6.0	Polar	Asp36, His81	Asp36, His81	88%
		Apolar	Asn20, His120, His122, Thr117, Trp41, Tyr80	Asn20, His120, His122, Thr117, Trp41	
6CC0	-7.3	Polar	Tyr66	Asp75, Ile77, Ile110, Met127, Phe54, Ser38, Thr72, Trp90, Tyr58, Tyr66, Val78	92%
		Apolar	Asp75, Ile77, Ile110, Met127, Phe54, Ser38, Ser129, Thr72, Trp62, Trp90, Tyr58, Val78		
4G4K	-5.0	Polar	Asp158, Asp176, Glu163, His174, His227,	Asp158, Asp176, Leu175, Tyr229	50%
		Apolar			

			Leu175, Phe161, Tyr229		
4BXI	-5.1	Polar		Ile3, Ile8, Ile20, Ile24, Leu5, Leu11, Lys17	88%
		Apolar	Ile3, Ile8, Ile20, Ile24, Ile36, Leu5, Leu11, Lys17		

*Fatty acids versus control

Table 3. Validation of molecular docking.

Figure 4 shows the binding affinities for the docking complexes due to the protonation states for each ligand (*e.g.*, protonated fatty acid *versus* deprotonated fatty acid) and with respect to the 1RO5, 3IT7, 6CC0, 4G4K and 4BXI proteins. As noted in Figure 5, in most situations, there is a decrease in binding affinity when the fatty acid is deprotonated, except in the analysis involving the 1RO5 protein, where the docking related to 1RO5 displayed greater values for the deprotonated states of oleic and palmitic acids. Such exceptions might be related to the carbon chain size and its influence on the interaction with the 1RO5 protein, as these fatty acids have a greater quantity of carbon compared to the others. In the case of the 4G4K protein, fatty acid deprotonation also led to decreased binding affinities in the protein-ligand complexes. This tendency also happened in the case of the 4BXI protein, with the exception of the interaction with oleic acid (which differs from the other fatty acids as it has an unsaturated carbon chain). For the 4BXI-oleic acid interaction, fatty acid deprotonation led to an increase in binding affinities.

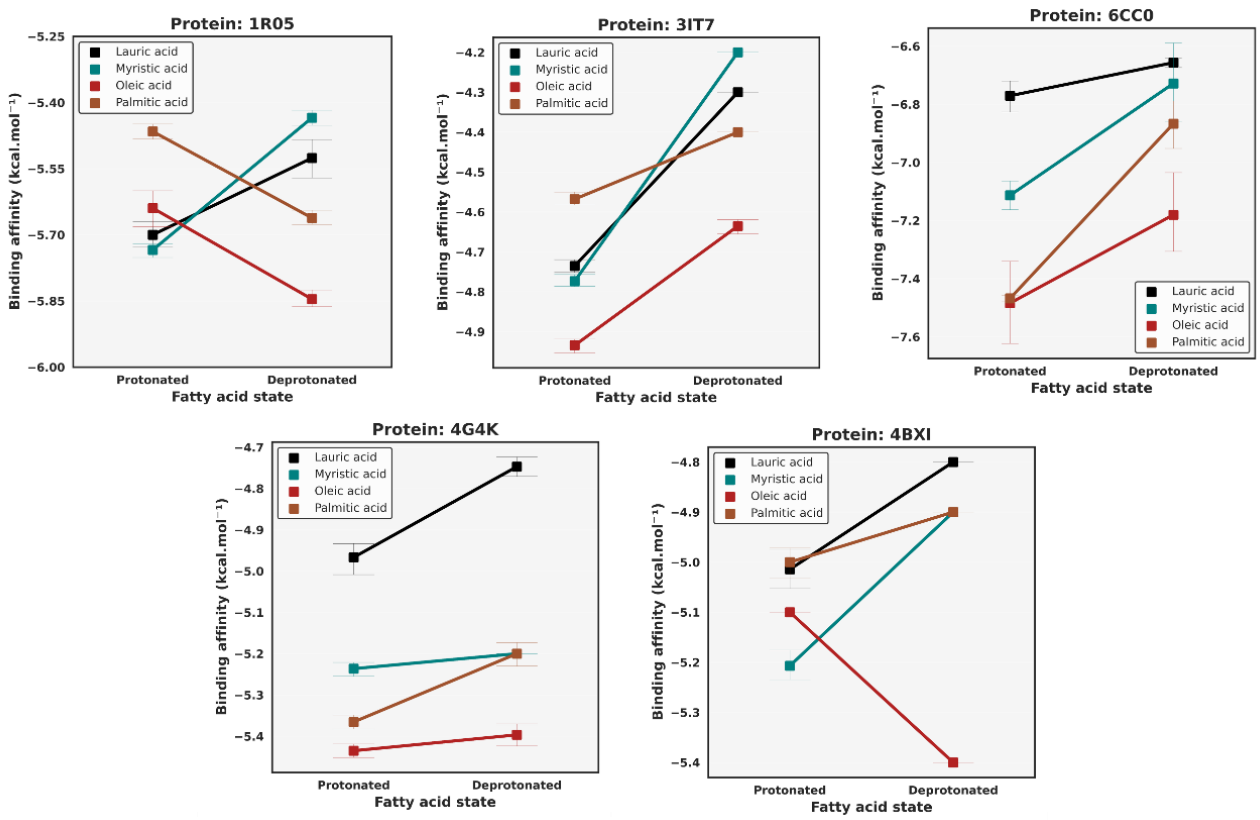

Figure 4. Binding affinities for the studied *docking* complexes due to fatty acid's protonation state.

Table 4 – Descriptive statistics for the aminoacid residues involved in docking.

Protein	Total number of residues	Unique residues	Mode	Frequency	Fatty acid state
1R05	137	18	Val143	13	Protonated
	111	18	Phe105	11	Deprotonated
3IT7	121	15	Trp41	12	Protonated
	95	19	Tyr151	10	Deprotonated
6CC0	192	28	Tyr66	12	Protonated
	186	27	Asp75	11	Deprotonated
4G4K	119	18	Tyr229	12	Protonated
	98	16	Asp158	11	Deprotonated
4BXI	113	13	Leu25	11	Protonated
	111	12	Lys17	12	Deprotonated

Based on the previous results, Table 4 shows some descriptive statistics for the amino acid residues involved in the molecular docking analyses. From a broad viewpoint, it is possible to note alterations in the nature of the protein-ligand interactions, justifying the differences in binding affinity values. The fatty acid

deprotonation interferes with the interacting amino acid residues during docking, which is exemplified by the change in the most frequent amino acid residue (the statistical mode) in each state (protonated *versus* deprotonated) – also shown in Table 4.

Although the majority of amino acid residues stayed constant during the interaction with each protein, the ligand deprotonation might induce differences in the type of interaction between the ligand and protein's amino acid residues (*e.g.*, polar and nonpolar contacts). As the binding affinity of the protein-ligand complexes depends on polar and nonpolar contacts (seen earlier in Equation 2), differences in the nature of the interaction could result in differences in binding affinity values. Figure 5 shows the influence of the fatty acid protonation state on the protein-ligand interactions, where the influence was evaluated through contingency tables, visually expressed as heatmaps.

The Chi-Squared test was used to statistically validate such a hypothesis, with a 95% confidence interval. Basically, the Chi-Squared test served to verify whether there was a relationship between the fatty acid protonation state and the change in proportion of the polar/nonpolar contacts to the amino acid residues of the studied proteins. In the case of 1RI5 ($p = 0.02520$), 6CC0 ($p = 0.00399$), 4G4K ($p = 0.02809$) and 4BXI ($p = 0.02888$) proteins, deprotonation of the fatty acids led to an increase in nonpolar interactions and, consequently, a decrease in polar interactions. However, for the 3IT7 protein, there was no relationship between the change in polar/nonpolar interactions and the protonation state of the fatty acids ($p = 0.22301$). Thus, the decrease in binding affinities of the protein-ligand complex when the fatty acid is deprotonated is explained by a modification of the nature of interactions in the analyses involving the 1RO5, 6CC0, 4G4K and 4BXI proteins, but this does not apply to the 3IT7 protein.

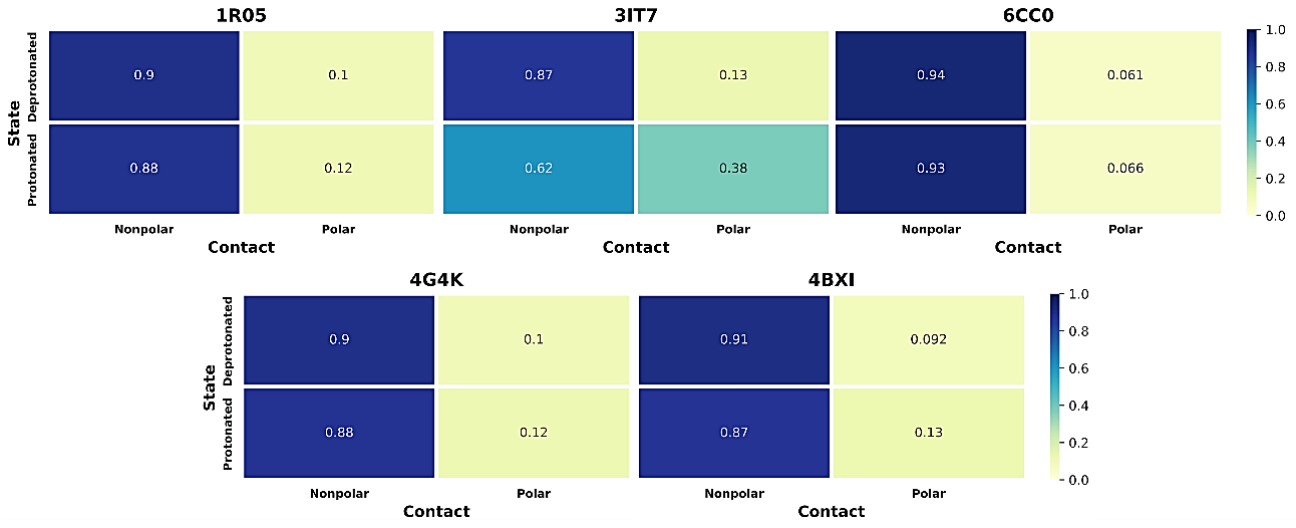

Figure 5 – Influence of fatty acid's protonation state on the protein-ligand interactions.

It is assumed that the binding affinity differences between the protein-ligand complexes for the 3IT7 protein were due to the contribution of five new amino acid residues (Gly27, Gly118, Pro42, Thr26 and Tyr117), which only occurred when the ligands were deprotonated. In the case of 6CC0, 4G4K and 4BXI proteins, only

a few new amino acid residues arose when the ligands were deprotonated, with one (Val126), two (Asp58, Cys228) and one (Ile38) new contributing amino acid residues for the deprotonated ligands of 6CC0, 4G4K and 4BXI proteins, respectively. There were no new contributing amino acids for the 1RO5 protein when the ligands were deprotonated.

In view of the results obtained from molecular docking, it is expected that the major fatty acids of tucumã oil and butter might present antimicrobial and/or antibiofilm activity against *P. aeruginosa* and *S. aureus* bacteria due to their binding affinity to the QS proteins of these microorganisms (Chakraborty et al., 2018; Kwiatkowski et al., 2019). Despite differences, these affinities occur for both protonated and deprotonated fatty acids. Oleic acid displayed the greatest binding affinities among all the studied fatty acids when considering the proteins of both bacteria.

4. Conclusion

The interaction of BNC with the major fatty acids of tucumã oil and butter was investigated through *ab initio* and molecular docking simulations in this paper. According to the simulation results, it is possible to modify/impregnate the BNC with tucumã oil and butter, and these modifying substances could potentially promote QQ of *P. aeruginosa* and *S. aureus*. The *ab initio* results suggest that the interaction of BNC with the tucumã oil and butter was through the physical adsorption of tucumã oil/butter major fatty acids over the cellulose matrix (represented by a cellobiose unit, in accordance with other DFT studies). The physical adsorption between cellobiose and each fatty acid is characterized as a reversible process, which could be reverted by physical stimuli, like temperature, pressure, humidity, pH and so forth. Moreover, the release of these major fatty acids might be used as a potential antimicrobial and/or antibiofilm agent, as the binding affinity to QS proteins of *P. aeruginosa* (gram-negative) and *S. aureus* (gram-positive) bacteria was observed through molecular docking. Both protonated and deprotonated forms of the fatty acids presented good binding affinity to 1RO5, 3IT7, 6CC0, 4G4K and 4XBI QS proteins. The deprotonation of the studied fatty acids tended to decrease the binding affinity between the protein-ligand complexes in mostly cases, and this was related to changes in the polar and nonpolar contacts during docking or to the rise of new interacting amino acid residues in the deprotonated state of the studied fatty acids. Among the fatty acids involved in this research, oleic acid displayed the greatest binding affinities when taking all the bacteria and proteins into account and its deprotonation had less influence on the binding affinity. In view of all this, a system composed of BNC and tucumã oil/butter could be used as raw biomaterial to produce chronic wound dressings. As a future perspective, the authors aim to experimentally validate the computational results of this research.

5. Acknowledgement

The authors would like to acknowledge interaction UFN (Universidade Franciscana) and CENAPAD-SP (Centro Nacional de Processamento de Alto Desempenho em São Paulo) for computer time and the Brazilian agencies CNPQ and CAPES for financial support.

6. References

Abol-Fotouh, D., Hassan, M. A., Shokry, H., Roig, A., Azab, M. S., & Kashyout, A. E.-H. B. (2020). Bacterial nanocellulose from agro-industrial wastes: low-cost and enhanced production by Komagataeibacter saccharivorans MD1. *Scientific Reports*, *10*(1), 3491. https://doi.org/10.1038/s41598-020-60315-9

An, S. qi, Murtagh, J., Twomey, K. B., Gupta, M. K., O'Sullivan, T. P., Ingram, R., … Tang, J. liang. (2019). Modulation of antibiotic sensitivity and biofilm formation in Pseudomonas aeruginosa by interspecies signal analogues. *Nature Communications*, *10*(1), 2334. https://doi.org/10.1038/s41467-019-10271-4

Arrigoni, M., & Madsen, G. K. H. (2019). Comparing the performance of LDA and GGA functionals in predicting the lattice thermal conductivity of III-V semiconductor materials in the zincblende structure: The cases of AlAs and BAs. *Computational Materials Science*, *156*, 354–360. https://doi.org/10.1016/j.commatsci.2018.10.005

Aslanli, A., Lyagin, I., Stepanov, N., Presnov, D., & Efremenko, E. (2020). Bacterial Cellulose Containing Combinations of Antimicrobial Peptides with Various QQ Enzymes as a Prototype of an "Enhanced Antibacterial" Dressing: In Silico and In Vitro Data. *Pharmaceutics*, *12*(12), 1155. https://doi.org/10.3390/pharmaceutics12121155

Asokan, G., Ramadhan, T., Ahmed, E., & Sanad, H. (2019). WHO Global Priority Pathogens List: A Bibliometric Analysis of Medline-PubMed for Knowledge Mobilization to Infection Prevention and Control Practices in Bahrain. *Oman Medical Journal*, *34*(3), 184–193. https://doi.org/10.5001/omj.2019.37

Azeredo, H. M. C., Barud, H., Farinas, C. S., Vasconcellos, V. M., & Claro, A. M. (2019). Bacterial Cellulose as a Raw Material for Food and Food Packaging Applications. *Frontiers in Sustainable Food Systems*, *3*.

Bacakova, L., Zikmundova, M., Pajorova, J., Broz, A., Filova, E., Blanquer, A., … Sinica, A. (2020). Nanofibrous Scaffolds for Skin Tissue Engineering and Wound Healing Based on Synthetic Polymers. In *Applications of Nanobiotechnology* (pp. 1–30). London, UK: IntechOpen.

Badhe, Y., Gupta, R., & Rai, B. (2019). Structural and barrier properties of the skin ceramide lipid bilayer: a molecular dynamics simulation study. *Journal of Molecular Modeling*, *25*(5), 140. https://doi.org/10.1007/s00894-019-4008-5

Baldissera, M. D., Souza, C. F., Doleski, P. H., Grando, T. H., Sagrillo, M. R., da Silva, A. S., … Monteiro, S. G. (2017). Treatment with tucumã oil (Astrocaryum vulgare) for diabetic mice prevents changes in seric enzymes of the purinergic system: Improvement of immune system. *Biomedicine & Pharmacotherapy*, *94*, 374–379. https://doi.org/10.1016/j.biopha.2017.07.113

Born, M., & Oppenheimer, R. (1927). Zur Quantentheorie der Molekeln. *Annalen Der Physik*, *389*(20), 457–484. https://doi.org/10.1002/andp.19273892002

Boys, S. F., & Bernardi, F. (1970). The calculation of small molecular interactions by the differences of separate total energies. Some procedures with reduced errors. *Molecular Physics*, *19*(4), 553–566. https://doi.org/10.1080/00268977000101561

Bressa, N. R., Oviedo, V. R., Machado, A. M. B., Almeida, W. L. de, Volkmer, T. M., Santos, L. A. L. dos, … Rodrigues Junior, L. F. (2021). Incorporation of astrocaryum vulgare (tucuma) oil into PCL electrospun

fibers. *Polímeros*, *31*(3). https://doi.org/10.1590/0104-1428.20210056

Cai, J., Chen, X., Wang, X., Tan, Y., Ye, D., Jia, Y., … Yu, H. (2018). High-water-absorbing calcium alginate fibrous scaffold fabricated by microfluidic spinning for use in chronic wound dressings. *RSC Advances*, *8*(69), 39463–39469.

Cartron, M. L., England, S. R., Chiriac, A. I., Josten, M., Turner, R., Rauter, Y., … Foster, S. J. (2014). Bactericidal Activity of the Human Skin Fatty Acid *cis* -6-Hexadecanoic Acid on Staphylococcus aureus. *Antimicrobial Agents and Chemotherapy*, *58*(7), 3599–3609. https://doi.org/10.1128/AAC.01043-13

Casillas-Vargas, G., Ocasio-Malavé, C., Medina, S., Morales-Guzmán, C., Del Valle, R. G., Carballeira, N. M., & Sanabria-Ríos, D. J. (2021). Antibacterial fatty acids: An update of possible mechanisms of action and implications in the development of the next-generation of antibacterial agents. *Progress in Lipid Research*, *82*, 101093. https://doi.org/10.1016/j.plipres.2021.101093

Cavalcanti, L. M., Pinto, F. C. M., De Oliveira, G. M., Lima, S. V. C., de Andrade Aguiar, J. L., & Lins, E. M. (2017). Efficacy of bacterial cellulose membrane for the treatment of lower limbs chronic varicose ulcers: a randomized and controlled trial. *Revista Do Colegio Brasileiro de Cirurgioes*, *44*(1), 72–80. https://doi.org/10.1590/0100-69912017001011

Chakraborty, P., Daware, A. V., Kumari, M., Chatterjee, A., Bhattacharyya, D., Mitra, G., … Tribedi, P. (2018). Free tryptophan residues inhibit quorum sensing of Pseudomonas aeruginosa: a potential approach to inhibit the development of microbial biofilm. *Archives of Microbiology*, *200*(10), 1419–1425. https://doi.org/10.1007/s00203-018-1557-4

Chemmugil, P., Lakshmi, P. T. V., & Annamalai, A. (2019). Exploring Morin as an anti-quorum sensing agent (anti-QSA) against resistant strains of Staphylococcus aureus. *Microbial Pathogenesis*, *127*, 304–315. https://doi.org/10.1016/J.MICPATH.2018.12.007

Choi, S. M., & Shin, E. J. (2020). The Nanofication and Functionalization of Bacterial Cellulose and Its Applications. *Nanomaterials*, *10*(3), 406. https://doi.org/10.3390/nano10030406

Cordenonsi, L. M., Santer, A., Sponchiado, R. M., Wingert, N. R., Raffin, R. P., & Schapoval, E. E. S. (2020). Amazonia Products in Novel Lipid Nanoparticles for Fucoxanthin Encapsulation. *AAPS PharmSciTech*, *21*(1), 32. https://doi.org/10.1208/s12249-019-1601-y

Cortes, E., Márquez, E., Mora, J. R., Puello, E., Rangel, N., De Moya, A., & Trilleras, J. (2019). Theoretical Study of the Adsorption Process of Antimalarial Drugs into Acrylamide-Base Hydrogel Model Using DFT Methods: The First Approach to the Rational Design of a Controlled Drug Delivery System. *Processes 2019, Vol. 7, Page 396*, *7*(7), 396. https://doi.org/10.3390/PR7070396

COSTA, B. E. T., SANTOS, O. V. dos, CORRÊA, N. C. F., & FRANÇA, L. F. de. (2016). Comparative study on the quality of oil extracted from two tucumã varieties using supercritical carbon dioxide. *Food Science and Technology*, *36*(2), 322–328. https://doi.org/10.1590/1678-457X.0094

Cresti, A., Lopez-Bezanilla, A., Ordejón, P., & Roche, S. (2011). Oxygen Surface Functionalization of Graphene Nanoribbons for Transport Gap Engineering. *ACS Nano*, *5*(11), 9271–9277. https://doi.org/10.1021/nn203573y

de Moraes, E. E., Tonel, M. Z., Fagan, S. B., & Barbosa, M. C. (2019). Density functional theory study of π-

aromatic interaction of benzene, phenol, catechol, dopamine isolated dimers and adsorbed on graphene surface. *Journal of Molecular Modeling*, *25*(10), 302. https://doi.org/10.1007/s00894-019-4185-2

de Oliveira, P. V., Goulart, L., Dos Santos, C. L., Rossato, J., Fagan, S. B., Zanella, I., … González-Durruthy, M. (2020). Computational Modeling of Environmental Co-exposure on Oil-Derived Hydrocarbon Overload by Using Substrate-Specific Transport Protein (TodX) with Graphene Nanostructures. *Current Topics in Medicinal Chemistry*, *20*(25), 2308–2325. https://doi.org/10.2174/1568026620666200820145412

De Salvi, D. T. B., da S. Barud, H., Treu-Filho, O., Pawlicka, A., Mattos, R. I., Raphael, E., & Ribeiro, S. J. L. (2014). Preparation, thermal characterization, and DFT study of the bacterial cellulose. *Journal of Thermal Analysis and Calorimetry*, *118*(1), 205–215. https://doi.org/10.1007/s10973-014-3969-y

Deka, B. C., & Bhattacharyya, P. K. (2017). DFT study on host-guest interaction in chitosan–amino acid complexes. *Computational and Theoretical Chemistry*, *1110*, 40–49. https://doi.org/10.1016/j.comptc.2017.03.036

Dow, M., & Naughton, L. M. (2017). Amphiphilic Lipids, Signaling Molecules, and Quorum Sensing. In *Cellular Ecophysiology of Microbe* (pp. 1–19). Cham: Springer International Publishing. https://doi.org/10.1007/978-3-319-20796-4_31-1

El-Wakil, N. A., Hassan, E. A., Hassan, M. L., & El-Salam, S. S. A. (2019). Bacterial cellulose/phytochemical's extracts biocomposites for potential active wound dressings. *Environmental Science and Pollution Research*, *26*(26), 26529–26541.

Espinosa-Urgel, M. (2016). Fatty Acids as Mediators of Intercellular Signaling. In *Cellular Ecophysiology of Microbe* (pp. 1–13). Cham: Springer International Publishing. https://doi.org/10.1007/978-3-319-20796-4_7-1

Feinstein, W. P., & Brylinski, M. (2015). Calculating an optimal box size for ligand docking and virtual screening against experimental and predicted binding pockets. *Journal of Cheminformatics*, *7*(1), 18. https://doi.org/10.1186/s13321-015-0067-5

Fernandes, C. P. (2015). Development of Nanoemulsions with Tucumã (Astrocaryum vulgare) Fruits Oil. *Journal of Nanomedicine Research*, *2*(2), 1–4. https://doi.org/10.15406/jnmr.2015.02.00024

Forli, S., Huey, R., Pique, M. E., Sanner, M. F., Goodsell, D. S., & Olson, A. J. (2016). Computational protein–ligand docking and virtual drug screening with the AutoDock suite. *Nature Protocols 2016 11:5*, *11*(5), 905–919. https://doi.org/10.1038/nprot.2016.051

Frykberg, R. G., & Banks, J. (2015). Challenges in the Treatment of Chronic Wounds. *Advances in Wound Care*, *4*(9), 560–582. https://doi.org/10.1089/wound.2015.0635

Gethin, G. (2007). The significance of surface pH in chronic wounds. *Wounds*, *3*(3), 52–56.

Gnanendra, S., Anusuya, S., & Natarajan, J. (2012). Molecular modeling and active site analysis of SdiA homolog, a putative quorum sensor for Salmonella typhimurium pathogenecity reveals specific binding patterns of AHL transcriptional regulators. *Journal of Molecular Modeling*, *18*(10), 4709–4719. https://doi.org/10.1007/s00894-012-1469-1

Gorgieva, S. (2020). Bacterial Cellulose as a Versatile Platform for Research and Development of Biomedical

Materials. *Processes*, *8*(5), 1–26.

Gould, A., Schweizer, H. P., Churchill, M. E. A., Gould, T. A., Schweizer, H. P., & Churchill, M. E. A. (2004). Structure of the Pseudomonas aeruginosa acyl-homoserinelactone synthase LasI. *Molecular Microbiology*, *53*(4), 1135–1146. https://doi.org/10.1111/J.1365-2958.2004.04211.X

Gould, L., Abadir, P., Brem, H., Carter, M., Conner-Kerr, T., Davidson, J., … Schmader, K. (2015). Chronic Wound Repair and Healing in Older Adults: Current Status and Future Research. *Journal of the American Geriatrics Society*, *63*(3), 427. https://doi.org/10.1111/JGS.13332

Hema, K., Ahamad, S., Joon, H. K., Pandey, R., & Gupta, D. (2021). Atomic resolution homology models and molecular dynamics simulations of plasmodium falciparum tubulins. *ACS Omega*, *6*(27), 17510–17522. https://doi.org/10.1021/ACSOMEGA.1C01988/SUPPL_FILE/AO1C01988_SI_001.PDF

Hernández Rosas, J. J., Ramírez Gutiérrez, R. E., Escobedo-Morales, A., & Chigo Anota, E. (2011). First principles calculations of the electronic and chemical properties of graphene, graphane, and graphene oxide. *Journal of Molecular Modeling*, *17*(5), 1133–1139. https://doi.org/10.1007/s00894-010-0818-1

Hohenberg, P., & Kohn, W. (1964). Inhomogeneous Electron Gas. *Physical Review*, *136*(3B), B864–B871. https://doi.org/10.1103/PhysRev.136.B864

Homaeigohar, S., & Boccaccini, A. R. (2020). Antibacterial biohybrid nanofibers for wound dressings. *Acta Biomaterialia*, *107*, 25–49.

Huang, J., Shi, Y., Zeng, G., Gu, Y., Chen, G., Shi, L., … Zhou, J. (2016). Acyl-homoserine lactone-based quorum sensing and quorum quenching hold promise to determine the performance of biological wastewater treatments: An overview. *Chemosphere*, *157*, 137–151. https://doi.org/10.1016/j.chemosphere.2016.05.032

Ituen, E. B., Essien, E. A., Udo, U. E., & Oluwaseyi, O. R. (2014). Experimental and theoretical study of corrosion inhibition effect of Cucumeropsis mannii N. seed oil metallic soap of zinc on mild steel surface in sulphuric acid. *Advances in Applied Science Researcha*, *5*(3), 1–28.

Jauris, I. M., Matos, C. F., Saucier, C., Lima, E. C., Zarbin, A. J. G., Fagan, S. B., … Zanella, I. (2016). Adsorption of sodium diclofenac on graphene: a combined experimental and theoretical study. *Physical Chemistry Chemical Physics*, *18*(3), 1526–1536. https://doi.org/10.1039/C5CP05940B

Jauris, Iuri M., Fagan, S. B., Adebayo, M. A., & Machado, F. M. (2016). Adsorption of acridine orange and methylene blue synthetic dyes and anthracene on single wall carbon nanotubes: A first principle approach. *Computational and Theoretical Chemistry*, *1076*, 42–50. https://doi.org/10.1016/j.comptc.2015.11.021

Jean-Quartier, C., Jeanquartier, F., Jurisica, I., & Holzinger, A. (2018). In silico cancer research towards 3R. *BMC Cancer*, *18*(1). https://doi.org/10.1186/S12885-018-4302-0

Jones, E. M., Cochrane, C. A., & Percival, S. L. (2015). The Effect of pH on the Extracellular Matrix and Biofilms. *Advances in Wound Care*, *4*(7), 431–439. https://doi.org/10.1089/wound.2014.0538

Jozala, A. F., de Lencastre-Novaes, L. C., Lopes, A. M., de Carvalho Santos-Ebinuma, V., Mazzola, P. G., Pessoa-Jr, A., … Chaud, M. V. (2016). Bacterial nanocellulose production and application: a 10-year overview. *Applied Microbiology and Biotechnology*, *100*(5), 2063–2072. https://doi.org/10.1007/s00253-015-7243-4

Kanikireddy, V., Varaprasad, K., Jayaramudu, T., Karthikeyan, C., & Sadiku, R. (2020). Carboxymethyl cellulose-based materials for infection control and wound healing: A review. *International Journal of Biological Macromolecules*, *164*, 963–975.

Kapil, J., Shukla, P., & Pathak, A. (2020). Review Article on Density Functional Theory. In *Springer Proceedings in Physics* (Vol. 256, pp. 211–220). Springer, Singapore. https://doi.org/10.1007/978-981-15-8625-5_22

Kecili, R., & Hussain, C. M. (2018). Mechanism of Adsorption on Nanomaterials. In *Nanomaterials in Chromatography* (pp. 89–115). Elsevier. https://doi.org/10.1016/B978-0-12-812792-6.00004-2

Kohn, W., & Sham, L. J. (1965). Self-Consistent Equations Including Exchange and Correlation Effects. *Physical Review*, *140*(4A), A1133–A1138. https://doi.org/10.1103/PhysRev.140.A1133

Kondo, T., Rytczak, P., & Bielecki, S. (2016). Bacterial NanoCellulose Characterization. *Bacterial Nanocellulose: From Biotechnology to Bio-Economy*, 59–71. https://doi.org/10.1016/B978-0-444-63458-0.00004-4

Kumar, P., Lee, J.-H., Beyenal, H., & Lee, J. (2020). Fatty Acids as Antibiofilm and Antivirulence Agents. *Trends in Microbiology*, *28*(9), 753–768.

Kwiatkowski, P., Pruss, A., Masiuk, H., Mnichowska-Polanowska, M., Kaczmarek, M., Giedrys-Kalemba, S., … Sienkiewicz, M. (2019). The effect of fennel essential oil and trans-anethole on antibacterial activity of mupirocin against Staphylococcus aureus isolated from asymptomatic carriers. *Postepy Dermatologii i Alergologii*, *36*(3), 308–314. https://doi.org/10.5114/ada.2018.76425

Lalouckova, K., Skrivanova, E., Rondevaldova, J., Frankova, A., Soukup, J., & Kokoska, L. (2021). In vitro antagonistic inhibitory effects of palm seed crude oils and their main constituent, lauric acid, with oxacillin in Staphylococcus aureus. *Scientific Reports*, *11*(1), 1–12. https://doi.org/10.1038/s41598-020-80481-0

Leonard, P. G., Bezar, I. F., Sidote, D. J., & Stock, A. M. (2012). Identification of a hydrophobic cleft in the LytTR domain of AgrA as a locus for small molecule interactions that inhibit DNA binding. *Biochemistry*, *51*(50), 10035–10043. https://doi.org/10.1021/BI3011785/ASSET/IMAGES/MEDIUM/BI-2012-011785_0006.GIF

Leonardi, B., Arauz, L. J. De, & Baruque-Ramos, J. (2019). Chemical characterization of Amazonian non-polar vegetal extracts (buriti, tucumã, Brazil nut, cupuaçu, and cocoa) by infrared spectroscopy (FTIR) and gas chromatography (GC-FID). *Infarma - Ciências Farmacêuticas*, *31*(3), 163–176.

Li, B., Ou, P., Wei, Y., Zhang, X., & Song, J. (2018). Polycyclic Aromatic Hydrocarbons Adsorption onto Graphene: A DFT and AIMD Study. *Materials*, *11*(5), 726. https://doi.org/10.3390/ma11050726

Li, Y., Lin, M., & Davenport, J. W. (2011). Ab Initio Studies of Cellulose I: Crystal Structure, Intermolecular Forces, and Interactions with Water. *The Journal of Physical Chemistry C*, *115*(23), 11533–11539. https://doi.org/10.1021/jp2006759

Lim, G.-H., Singhal, R., Kachroo, A., & Kachroo, P. (2017). Fatty Acid– and Lipid-Mediated Signaling in Plant Defense. *Annual Review of Phytopathology*, *55*(1), 505–536. https://doi.org/10.1146/annurev-phyto-080516-035406

Lopreiato, M., Di Cristofano, S., Cocchiola, R., Mariano, A., Guerrizio, L., Scandurra, R., … Scotto d'Abusco, A. (2021). Biochemical and Computational Studies of the Interaction between a Glucosamine Derivative, NAPA, and the IKKα Kinase. *International Journal of Molecular Sciences*, *22*(4), 1643. https://doi.org/10.3390/ijms22041643

Machado, F. M., Carmalin, S. A., Lima, E. C., Dias, S. L. P., Prola, L. D. T., Saucier, C., … Fagan, S. B. (2016). Adsorption of Alizarin Red S Dye by Carbon Nanotubes: An Experimental and Theoretical Investigation. *The Journal of Physical Chemistry C*, *120*(32), 18296–18306. https://doi.org/10.1021/acs.jpcc.6b03884

Miar, M., Shiroudi, A., Pourshamsian, K., Oliaey, A. R., & Hatamjafari, F. (2021). Theoretical investigations on the HOMO–LUMO gap and global reactivity descriptor studies, natural bond orbital, and nucleus-independent chemical shifts analyses of 3-phenylbenzo[*d*]thiazole-2(3 *H*)-imine and its *para* -substituted der. *Journal of Chemical Research*, *45*(1–2), 147–158. https://doi.org/10.1177/1747519820932091

Moghadam, M. T., Khoshbayan, A., Chegini, Z., Farahani, I., & Shariati, A. (2020). Bacteriophages, a New Therapeutic Solution for Inhibiting Multidrug-Resistant Bacteria Causing Wound Infection: Lesson from Animal Models and Clinical Trials. *Drug Design, Development and Therapy*, *Volume 14*, 1867–1883.

Mohammed, N. J., Othman, N. K., Taib, M. F. M., Samat, M. H., & Yahya, S. (2021). Experimental and Theoretical Studies on Extract of Date Palm Seed as a Green Anti-Corrosion Agent in Hydrochloric Acid Solution. *Molecules*, *26*(12), 1–18. https://doi.org/10.3390/molecules26123535

Nethi, S. K., Das, S., Patra, C. R., & Mukherjee, S. (2019). Recent advances in inorganic nanomaterials for wound-healing applications. *Biomaterials Science*, *7*(7), 2652–2674.

Nogueira, J. R., Verza, F. A., Nishimura, F., Das, U., Caruso, Í. P., Fachin, A. L., Marins, M. (2021). Molecular Docking Studies of Curcumin Analogues against SARS-CoV-2 Spike Protein. *Journal of the Brazilian Chemical Society*, *32*(10), 1943–1955. https://doi.org/10.21577/0103-5053.20210085

Norrrahim, M. N. F., Nurazzi, N. M., Jenol, M. A., Farid, M. A. A., Janudin, N., Ujang, F. A., … Ilyas, R. A. (2021). Emerging development of nanocellulose as an antimicrobial material: an overview. *Materials Advances*, *2*(11), 3538–3551. https://doi.org/10.1039/D1MA00116G

Olsson, M., Järbrink, K., Divakar, U., Bajpai, R., Upton, Z., Schmidtchen, A., & Car, J. (2019). The humanistic and economic burden of chronic wounds: A systematic review. *Wound Repair and Regeneration*, *27*(1), 114–125. https://doi.org/10.1111/wrr.12683

Oviedo, V. R., Balbé, F. P., Rodrigues Jr., L. F., Sagrillo, M. R., Fagan, S. B., & Fernandes, L. da S. (2021). Bacterial nanocellulose membranes as potential chronic wound dressing: influence of alternative culture media on nanofiber diameter - a brief review. *Disciplinarum Scientia - Ciências Naturais e Tecnológicas*, *22*(3), 31–44. https://doi.org/10.37779/nt.v22i3.4091

Pang, M., Huang, Y., Meng, F., Zhuang, Y., Liu, H., Du, M., Cai, Y. (2020). Application of bacterial cellulose in skin and bone tissue engineering. *European Polymer Journal*, *122*, 1–30.

Papenfort, K., & Bassler, B. L. (2016). Quorum sensing signal–response systems in Gram-negative bacteria. *Nature Reviews Microbiology*, *14*(9), 576–588. https://doi.org/10.1038/nrmicro.2016.89

Perdew, J. P., & Zunger, A. (1981). Self-interaction correction to density-functional approximations for many-

electron systems. *Physical Review B*, *23*(10), 5048. https://doi.org/10.1103/PhysRevB.23.5048

Pereira dos Santos, E., Nicácio, P. H. M., Coêlho Barbosa, F., Nunes da Silva, H., Andrade, A. L. S., Lia Fook, M. V., Farias Leite, I. (2019). Chitosan/Essential Oils Formulations for Potential Use as Wound Dressing: Physical and Antimicrobial Properties. *Materials*, *12*(14), 1–21. https://doi.org/10.3390/ma12142223

Pontoh, R., Rarisavitri, V. E., Yang, C. C., Putra, M. F., & Anugrah, D. S. B. (2022). Density Functional Theory Study of Intermolecular Interactions between Amylum and Cellulose. *Indonesian Journal of Chemistry*, *22*(1), 253. https://doi.org/10.22146/ijc.69241

Portela, R., Leal, C. R., Almeida, P. L., & Sobral, R. G. (2019). Bacterial cellulose: a versatile biopolymer for wound dressing applications. *Microbial Biotechnology*, *12*(4), 586–610.

Rahmawati, S., Radiman, C. L., & Martoprawiro, M. A. (2018). Density Functional Theory (DFT) and Natural Bond Orbital (NBO) Analysis of Intermolecular Hydrogen Bond Interaction in "Phosphorylated Nata De Coco - Water." *Indonesian Journal of Chemistry*, *18*(1), 173. https://doi.org/10.22146/ijc.25170

Ramos, P., Schmitz, M., Gama, S., Portantiolo, A., Durruthy, M. G., de Souza Votto, A. P., … Monserrat, J. M. (2018). Cytoprotection of lipoic acid against toxicity induced by saxitoxin in hippocampal cell line HT-22 through in silico modeling and in vitro assays. *Toxicology*, *393*, 171–184. https://doi.org/10.1016/j.tox.2017.11.004

Rehman, Z. U., & Leiknes, T. O. (2018). Quorum-quenching bacteria isolated from red sea sediments reduce biofilm formation by Pseudomonas aeruginosa. *Frontiers in Microbiology*, *9*(1354), 1–13. https://doi.org/10.3389/FMICB.2018.01354/BIBTEX

Rossato, A., Silveira, L. da S., Oliveira, P. S., Filho, W. P. de S., Wagner, R., Klein, B., … Sagrillo, M. R. (2020). Evaluation of anti-inflammatory and healing activity of a nano-structured lipid carrier containing tucuman butter oil and butter. *Disciplinarum Scientia - Ciências Naturais e Tecnológicas*, *21*(3), 99–108. https://doi.org/10.37779/nt.v21i3.3551

Rossato, A., Silveira, L. da S., Oliveira, P. S., Souza, T. T. de, Becker, A. P., Wagner, R., … Sagrillo, M. R. (2021). Safety profile, antimicrobial and antibiofilm activities of a nanostructured lipid carrier containing oil and butter from Astrocaryum vulgare: in vitro studies. *International Journal for Innovation Education and Research*, *9*(5), 478–497. https://doi.org/10.31686/ijier.vol9.iss5.3113

Ruiz-Morales, Y. (2002). HOMO−LUMO Gap as an Index of Molecular Size and Structure for Polycyclic Aromatic Hydrocarbons (PAHs) and Asphaltenes: A Theoretical Study. I. *Journal of Physical Chemistry A*, *106*(46), 11283–11308. https://doi.org/10.1021/JP021152E

SALIHU, R., FOONG, C. Y. E. E., RAZAK, S. I. A. B. D., KADIR, M. R. A., YUSOF, A. H. M., & NAYAN, G. H. M. A. T. (2019). Overview of inexpensive production routes of bacterial cellulose and its applications in biomedical engineering. *Cellulose Chemistry and Technology*, *53*(1–2), 1–13.

Santos, J. G. S., Macedo-Filho, A., Silva, A. M., de Sousa, F. F., Caetano, E. W. S., da Silva, M. B., & Freire, V. N. (2021). Computational structural, electronic and optical properties of the palmitic acid in its C form. *Journal of Molecular Modeling*, *27*(5), 145. https://doi.org/10.1007/s00894-021-04752-x

Schopf, P. F., Zanella, I., Cordeiro, M. N. D. S., Ruso, J. M., González-Durruthy, M., & Martins, M. O. (2021). Nanomarker for Early Detection of Alzheimer's Disease Combining Ab initio DFT Simulations and

Molecular Docking Approach. *Biophysica 2021, Vol. 1, Pages 76-86*, *1*(2), 76–86. https://doi.org/10.3390/BIOPHYSICA1020007

Schweiker, S. S., & Levonis, S. M. (2020). Navigating the intricacies of molecular docking. *Future Medicinal Chemistry*, *12*(6), 469–471. https://doi.org/10.4155/fmc-2019-0355

Sekar, P. C., Paul, D. M., Srinivasan, E., & Rajasekaran, R. (2021). Unravelling the molecular effect of ocellatin-1, F1, K1 and S1, the frog-skin antimicrobial peptides to enhance its therapeutics—quantum and molecular mechanical approaches. *Journal of Molecular Modeling*, *27*(1), 10. https://doi.org/10.1007/s00894-020-04652-6

Shahi, S. K., Singh, V. K., Kumar, A., Gupta, S. K., & Singh, S. K. (2013). Interaction of dihydrofolate reductase and aminoglycoside adenyltransferase enzyme from Klebsiella pneumoniae multidrug resistant strain DF12SA with clindamycin: a molecular modelling and docking study. *Journal of Molecular Modeling*, *19*(3), 973–983. https://doi.org/10.1007/s00894-012-1635-5

Shoemark, D. K., Colenso, C. K., Toelzer, C., Gupta, K., Sessions, R. B., Davidson, A. D., Mulholland, A. J. (2021). Molecular Simulations suggest Vitamins, Retinoids and Steroids as Ligands of the Free Fatty Acid Pocket of the SARS-CoV-2 Spike Protein. *Angewandte Chemie International Edition*, *60*(13), 7098–7110. https://doi.org/10.1002/anie.202015639

Soler, J. M., Artacho, E., Gale, J. D., García, A., Junquera, J., Ordejón, P., & Sánchez-Portal, D. (2002). The SIESTA method for *ab initio* order- *N* materials simulation. *Journal of Physics: Condensed Matter*, *14*(11), 2745–2779. https://doi.org/10.1088/0953-8984/14/11/302

Stumpf, T. R., Yang, X., Zhang, J., & Cao, X. (2018). In situ and ex situ modifications of bacterial cellulose for applications in tissue engineering. *Materials Science and Engineering: C*, *82*, 372–383.

Subramani, R., & Jayaprakashvel, M. (2019). Bacterial Quorum Sensing: Biofilm Formation, Survival Behaviour and Antibiotic Resistance. In *Implication of Quorum Sensing and Biofilm Formation in Medicine, Agriculture and Food Industry* (pp. 21–37). Singapore: Springer Singapore. https://doi.org/10.1007/978-981-32-9409-7_3

Teixeira, M. A., Paiva, M. C., Amorim, M. T. P., & Felgueiras, H. P. (2020). Electrospun Nanocomposites Containing Cellulose and Its Derivatives Modified with Specialized Biomolecules for an Enhanced Wound Healing. *Nanomaterials*, *10*(3), 557. https://doi.org/10.3390/nano10030557

Tonel, M. Z., González-Durruthy, M., Zanella, I., & Fagan, S. B. (2019). Interactions of graphene derivatives with glutamate-neurotransmitter: A parallel first principles - Docking investigation. *Journal of Molecular Graphics and Modelling*, *88*, 121–127. https://doi.org/10.1016/j.jmgm.2019.01.007

Tournus, F., & Charlier, J.-C. (2005). Ab initio study of benzene adsorption on carbon nanotubes. *Physical Review B*, *71*(16), 165421. https://doi.org/10.1103/PhysRevB.71.165421

Tournus, F., Latil, S., Heggie, M. I., & Charlier, J.-C. (2005). π-stacking interaction between carbon nanotubes and organic molecules. *Physical Review B*, *72*(7), 075431. https://doi.org/10.1103/PhysRevB.72.075431

Trott, O., & Olson, A. J. (2009). AutoDock Vina: Improving the speed and accuracy of docking with a new scoring function, efficient optimization, and multithreading. *Journal of Computational Chemistry*, *31*(2), NA-NA. https://doi.org/10.1002/jcc.21334

Varier, K. M., Gudeppu, M., Chinnasamy, A., Thangarajan, S., Balasubramanian, J., Li, Y., & Gajendran, B. (2019). Nanoparticles: Antimicrobial Applications and Its Prospects. *Advanced Nanostructured Materials for Environmental Remediation*, *25*, 321. https://doi.org/10.1007/978-3-030-04477-0_12

Vilela, C., Freire, C. S. R., Araújo, C., Rudić, S., Silvestre, A. J. D., Vaz, P. D., Nolasco, M. M. (2020). Understanding the Structure and Dynamics of Nanocellulose-Based Composites with Neutral and Ionic Poly(methacrylate) Derivatives Using Inelastic Neutron Scattering and DFT Calculations. *Molecules*, *25*(7), 1–16. https://doi.org/10.3390/molecules25071689

Wang, K., Wang, F., Lou, Z., Han, Q., Zhao, Q., Hu, K., … Li, J. (2020). Relationship between the Electrical Characteristics of Molecules and Fast Streamers in Ester Insulation Oil. *International Journal of Molecular Sciences 2020, Vol. 21, Page 974*, *21*(3), 1–13. https://doi.org/10.3390/IJMS21030974

Wang, Y., Lu, Y., Zhang, J., Hu, X., Yang, Z., Guo, Y., & Wang, Y. (2019). A synergistic antibacterial effect between terbium ions and reduced graphene oxide in a poly(vinyl alcohol)-alginate hydrogel for treating infected chronic wounds. *Journal of Materials Chemistry B*, *7*(4), 538–547.

Xiao, Y., Ahadian, S., & Radisic, M. (2017). Biochemical and Biophysical Cues in Matrix Design for Chronic and Diabetic Wound Treatment. *Tissue Engineering Part B: Reviews*, *23*(1), 9–26.

Zarei, S., Niad, M., & Raanaei, H. (2018). The removal of mercury ion pollution by using Fe3O4-nanocellulose: Synthesis, characterizations and DFT studies. *Journal of Hazardous Materials*, *344*, 258–273. https://doi.org/10.1016/j.jhazmat.2017.10.009

Zhang, G., & Musgrave, C. B. (2007). Comparison of DFT methods for molecular orbital eigenvalue calculations. *Journal of Physical Chemistry A*, *111*(8), 1554–1561. https://doi.org/10.1021/

Zhang, X., Shu, W., Yu, Q., Qu, W., Wang, Y., & Li, R. (2020). Functional Biomaterials for Treatment of Chronic Wound. *Frontiers in Bioengineering and Biotechnology*, *8*, 516.

Appendix

Figure S1. LDOS charge density plots for the isolated structures (*isosurface values* of 0.001 e^-/$Borh^3$).

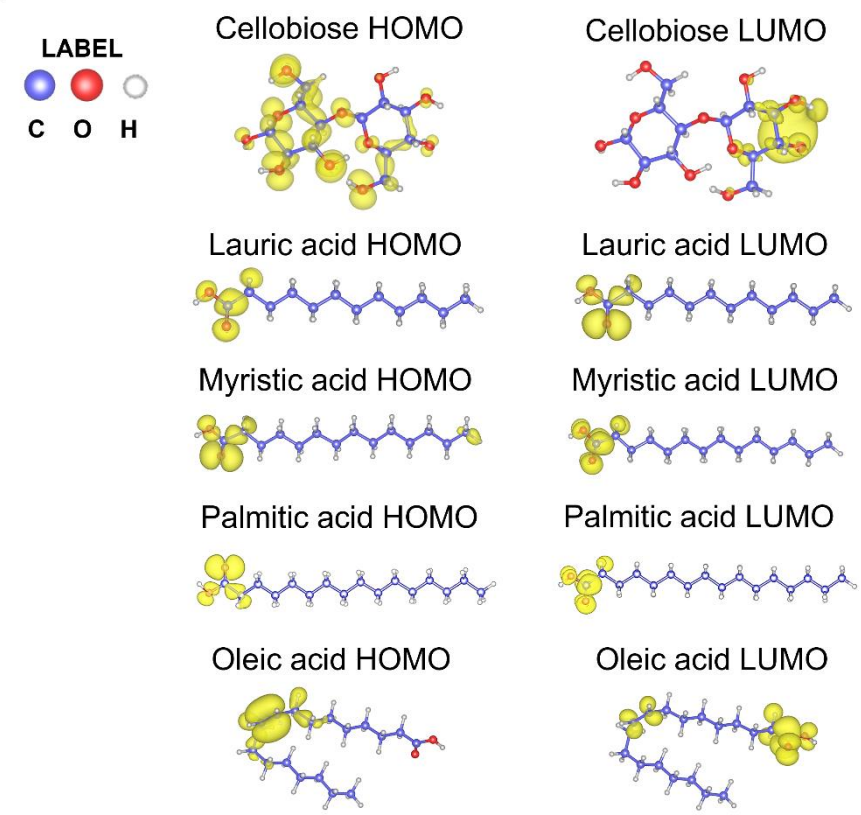
LABEL
C O H
Cellobiose HOMO
Cellobiose LUMO
Lauric acid HOMO
Lauric acid LUMO
Myristic acid HOMO
Myristic acid LUMO
Palmitic acid HOMO
Palmitic acid LUMO
Oleic acid HOMO
Oleic acid LUMO

Figure S2. Configurations for the interaction of cellobiose-myristic acid (CBM), cellobiose-palmitic acid (CBP) and cellobiose-oleic acid (CBO) systems.

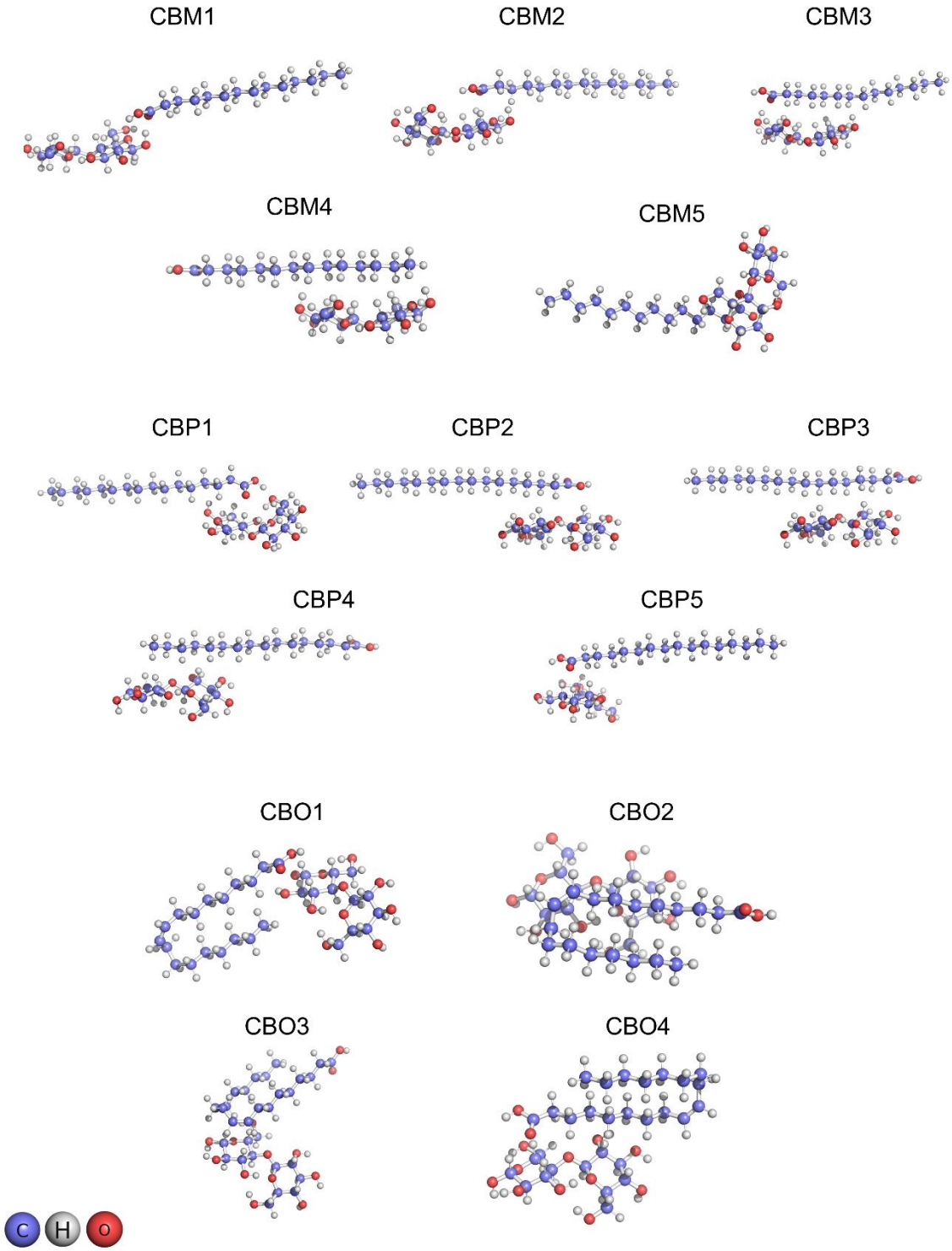

Figure S3. Energy levels and LDOS plots for the most stables systems of cellobiose-myristic acid and cellobiose palmitic acid (isosurface values of 0.001 e^-/Borh^3).

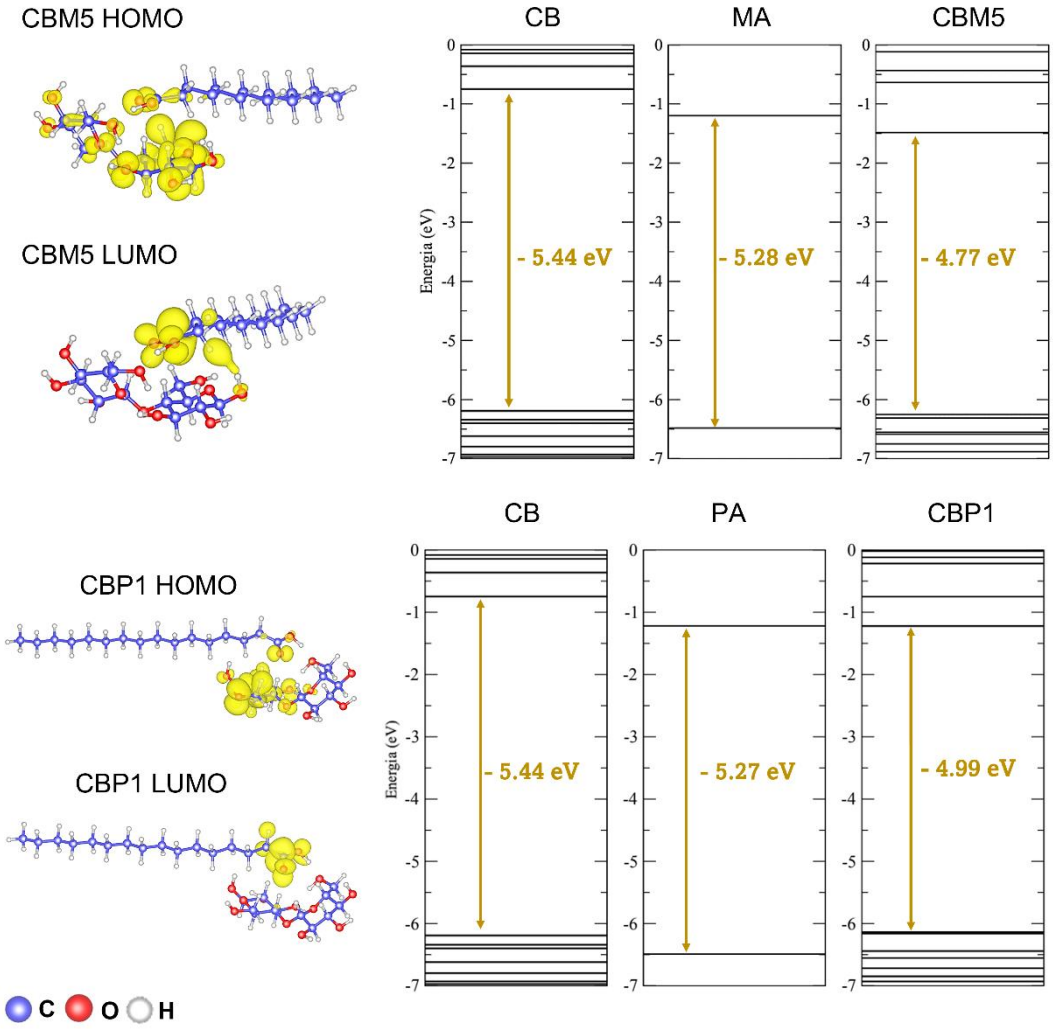

Figure S4. Ramachandran plot for 4BXI homologue protein (modeled through Swiss-Model).

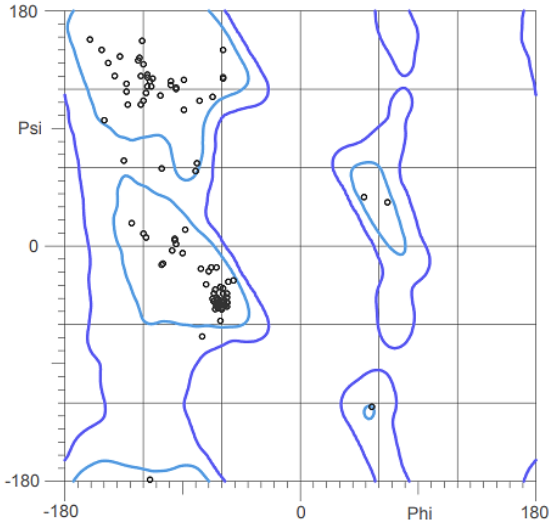

Table S1 – Docking grid box dimensions.

Protein/Ligand	Coordinates (x, y, z) – units in Å	Parameter

1RO5	(43.7, -14.1, -13.0)	Grid box center
3IT7	(26.2, 2.93, -5.57)	Grid box center
6CC0	(-77.1, -10.1, 13.5)	Grid box center
4G4K	(25.5, 28.3, 40.5)	Grid box center
4BXI	(-19.7, -3.7, -4.5)	Grid box center
Lauric acid	(21.252, 21.252, 21.252)	Grid box size
Myristic acid	(24.651, 24.651, 24.651)	Grid box size
Oleic acid	(19.236, 19.236, 19.236)	Grid box size
Palmitic acid	(27.988, 27.988, 27.988)	Grid box size

Table S2. Binding affinities of tucumã oil and butter major fatty acids against QS proteins of *Pseudomonas aeruginosa*.

Protein	Fatty acid	Protonated		Deprotonated	
		Conformation	Affinity (kcal.mol^{-1})	Conformation	Affinity (kcal.mol^{-1})
1RO5	Lauric acid	1	-5.8	1	-5.7
		2	-5.7	2	-5.5
		3	-5.6	3	-5.4
	Myristic acid	1	-5.8	1	-5.5
		2	-5.7	2	-5.4
		3	-5.7	3	-5.4
	Oleic acid	1	-5.8	1	-5.9
		2	-5.6	2	-5.8
		3	-5.5		
	Palmitic acid	1	-5.5	1	-5.7
		2	-5.5	2	-5.7
		3	-5.4	3	-5.6
3IT7	Lauric acid	1	-4.8	1	-4.3
		2	-4.7	2	-4.3
		3	-4.7	3	-4.3
	Myristic acid	1	-4.8	1	-4.2
		2	-4.8		
		3	-4.7		
	Oleic acid	1	-5.0	1	-4.7
		2	-4.9	2	-4.6
		3	-4.9	3	-4.6
	Palmitic acid	1	-4.6	1	-4.4
		2	-4.6	2	-4.4
		3	-4.5	3	-4.4
6CC0	Lauric acid	1	-7.0	1	-6.7
		2	-6.7	2	-6.6
		3	-6.6		
	Myristic acid	1	-7.3	1	-7.1
		2	-7.1	2	-7.0
		3	-6.9		
	Oleic acid	1	-8.2	1	-7.9

		2	-7.2	2	-7.0
		3	-6.9	3	-6.6
	Palmitic acid	1	-7.5	1	-7.3
		2	-7.5	2	-6.7
		3	-7.4	3	-6.3

Table S3 – Binding affinities of tucumã oil and butter major fatty acids against QS proteins of *Staphylococcus aureus*.

Protein	**Fatty acid**	**Protonated**		**Deprotonated**	
		Conformation	**Affinity (kcal.mol^{-1})**	**Conformation**	**Affinity (kcal.mol^{-1})**
4G4K	Lauric acid	1	-5.1	1	-4.8
		2	-4.9	2	-4.7
		3	-4.9		
	Myristic acid	1	-5.3	1	-5.2
		2	-5.2	2	-5.2
		3	-5.2	3	-5.2
	Oleic acid	1	-5.5	1	-5.5
		2	-5.4	2	-5.4
		3	-5.4	3	-5.3
	Palmitic acid	1	-5.4	1	-5.3
		2	-5.4	2	-5.2
		3	-5.3	3	-5.1
4BXI	Lauric acid	1	-5.1	1	-4.8
		2	-4.9	2	-4.8
		-		3	-4.8
	Myristic acid	1	-5.3	1	-4.9
		2	-5.2	2	-4.9
		3	-5.1	3	-4.9
	Oleic acid	1	-5.1	1	-5.4
		2	-5.1	2	-5.4
		3	-5.1	3	-5.4
	Palmitic acid	1	-5.1	1	-4.9
		2	-5.0	2	-4.9
		3	-4.9		